Measuring the Dynamics and Kinetics of OXA-58, a Class D β-Lactamase from *Acinetobacter baumannii*

Preet Kamal Singh Gill

A THESIS SUBMITTED TO
THE FACULTY OF GRADUATE STUDIES
IN PARTIAL FULFILLMENT OF THE REQUIREMENTS
FOR THE DEGREE OF
MASTER OF SCIENCE

GRADUATE PROGRAM IN CHEMISTRY
YORK UNIVERSITY
TORONTO, ONTARIO

June 2015

Abstract

OXA-58 is a β-lactamase enzyme that bacteria *Acinetobacter baumannii* employ as their chief defense mechanism against β-lactam antibiotic treatment. The catalytic activity of OXA-58 and its mutants was monitored as they turned over a series of β-lactam antibiotics. Isothermal titration calorimetry (ITC) showed that the mutation of phenylalanine114 to isoleucine (F114I) had the most detrimental impact on the catalytic efficiency of the enzyme. Isoleucine has a more branched side chain than phenylalanine, which lead to decreased substrate binding and a low catalytic efficiency of F114I mutant. A custom made microfluidic chip coupled to Hydrogen/deuterium exchange (HDX) mass spectrometry (MS) technique was used to study the dynamics of free enzyme and during its reactions with good substrate oxacillin and poor substrate imipenem. The conformational space that OXA-58 explores was constrained in the presence of substrate, suggestive of an induced fit model for catalysis-linked dynamics.

Acknowledgments

First of all I would like to express my gratitude towards my two research supervisors for giving me a chance to work in their wonderful laboratories. Without Dr. Dasantila Golemi-Kotra and Dr. Derek J. Wilson, completing this thesis would not have been possible.

Dr. Dasantila Golemi-Kotra was always present for inspirational guidance and critical insight throughout my research project. Her affection and support during the tough times is invaluable. She provided me with flexibility when I needed it and she was the individual that always kept me motivated and focused on the goal.

I highly appreciate Dr. Derek J. Wilson's critical insight and guidance throughout the course of my research term. He was always supportive of the decisions I took in terms of where the project was going and always stood by me. His affection during the times of struggle and tremendous advice are priceless.

Next I would like to thank all of the fine people that I have come to know and work with over the course of my term. It was because of these people that time flew by so fast. These include members of the Dr. Golemi-Kotra lab: Uzma Muzamal, Kevin Patel, Shamina Prova, Muhammad Rahman, Zhifeng Yang, Michael Fridman, Daniel Gomez and Martin Romero. From Dr. Wilson's group these members would be Tamanna Rob, Peter Liuni, Yanfang Liang, Shaolong Zhu, Declan Williams, John van Nostrand, Cristina Lento and Kerene Brown. I would especially like to show appreciation for Tamanna, Peter and Shaolong for sharing not only their mass spectrometry knowledge but also their precious time with me, which I hold close to my heart. Kevin was the individual I could go to for any questions I had regarding purification and we often shared trips to campus coffee shop.

Special thanks to Dr. Gerald F. Audette for his precious suggestions during my research evaluations. His contribution was key in me being able to write up my research project.

Last but not least, I am thankful that I have such loving parents who have always been kind and supportive, so much so that they'd sacrifice their own comfort for mine. This thesis is dedicated to my father Balvir Singh Gill and mother Satinder Kaur Gill. This is just as much their victory as it is mine.

Table of Contents

List of Tables

List of Figures

List of Abbreviations

CD – Circular dichroism

CHDL – Carbapenem-hydrolyzing Class D β-lactamase

D_2O – Deuterium oxide

Da – Dalton

DM – Double mutant of OXA-58

DTT – Dithiothreitol

ESI – Electrospray ionization

FPLC – Fast protein liquid chromatography

HDX – Hydrogen/deuterium exchange

HDX-MS – Hydrogen/deuterium exchange-Mass spectrometry

HSQC – Heteronuclear Single Quantum Coherence

IPTG – Isopropyl β-D-1-thiogalactopyranoside

ITC – Isothermal titration calorimetry

LB – Luria bertani

MCP – Micro-channel plate

MS – Mass spectrometry

NMR – Nuclear Magnetic Resonance

PBP – Penicillin binding protein

PMMA – Poly(methyl methacrylate)

Q-TOF – Quadrupole-time of flight

SDS – Sodium dodecyl sulfate

SDS-PAGE – Sodium dodecyl sulfate-polyacrylamide gel electrophoresis

SP – Sulfopropyl

TB – Terrific broth

TOF – Time of flight

TRESI-MS – Time-resolved electrospray ionization mass spectrometry

WT – Wild-type

Chapter 1

Introduction

1.1 *Acinetobacter baumannii*

First proposed by Brisou and Prévot in 1954, the genus name *Acinetobacter* became broadly accepted in 1968.[1-3] *Acinetobacter baumannii* is a gram-negative bacterium that is responsible for many community and health care-associated infections (HAIs) such as bloodstream, urinary tract, and surgical wound infections, targeting mostly the immunocompromised individuals.[4] Found almost everywhere in nature (water, soil, etc.), the bacteria have been also identified in living organisms like fleas and ticks, which is alarming as these small organisms can serve as easy carriers for the pathogenic species.[5] *A. baumannii* is a pathogen of concern due to its ability to thrive in variety of habitats (in temperatures ranging from 20-30 ºC on lab media and 37-42 ºC in clinical setting), its ability to mount up mechanisms of antimicrobial resistance, and its tendency to cause infectious outbreaks.[6,7]

1.1.1 Approach to fighting bacterial infections: β–lactam antibiotics

Synthesis of bacterial cell wall is vital for cell growth, division and maintenance of structure. Penicillin-binding proteins (PBPs), also known as DD-peptidases are the bacterial enzymes involved in transpeptidation reaction, whereby a D-alanine is removed from peptidoglycan precursor and then peptidoglycan chains are cross-linked in order to form firm cell walls.[8-10]

The most commonly used antibiotics against bacterial infections are β-lactam antibiotics, mainly because of their high specificity and effectiveness.[11-13] These compounds have a four-

membered cyclic amide ring in their chemical structure, called the β-lactam ring.[14-17] The structure of the β-lactam ring is similar to that of the D-alanyl-D-alanine backbone of peptidoglycan precursor on which the PBPs act.[16,17] β-lactams form stable covalent complexes with the PBPs in the active site because they mimic natural PBP substrates, thus inhibiting PBPs from carrying out normal cell wall synthesis.[16-19] This results in a weakened cell wall and selective permeability loss, which ultimately causes cell death.[16,19] The structures of antibiotics used in the experiments are provided in figure 1.1, which differ based on the type of ring fused to core β-lactam ring and the side chains branching from the rings.[13,14,20,21]

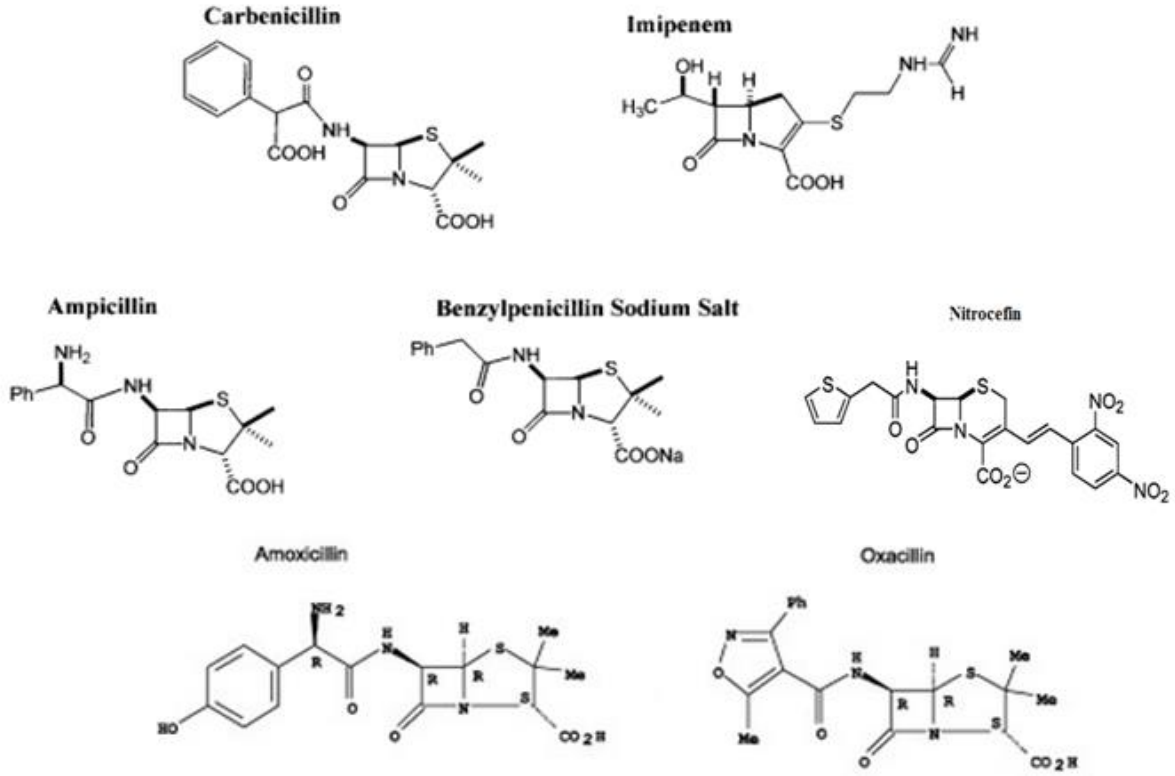

Figure 1.1 β-lactam antibiotics.[22-24] A class of antibiotic agents that have a cyclic amide ring called the β-lactam ring common in their structures.[14-17] The molecular structures vary in terms of the cyclic ring fused to the β-lactam ring, as well as the side chains that are attached to these rings.[13,14,20,21] The β-lactam antibiotics work by inhibiting bacterial proteins from carrying out cell wall synthesis.[16-19]

The carbapenem class of β-lactam antibiotics (ex. imipenem, meropenem) is known to be the most effective and sort of the last treatment option against *A. baumannii* infections.[25,26] However, now carbapenem-resistant *A. baumannii* has emerged all over the world.[26,27] This is a matter of utmost concern and requires an urgent action to develop new and effective treatments to combat antibiotic resistance.[27]

1.1.2 Antibiotic resistance in *Acinetobacter baumannii*: Production of β-lactamases

A broad range of resistance mechanisms exist inside *A. baumannii*, with hydrolysis of β-lactam antibiotics by β-lactamase enzymes being the most prominent one.[27-29] β-lactamases are enzymes produced by bacteria to combat the antibacterial properties of β-lactam antibiotics.[27-32] These enzymes essentially work by breaking open the β-lactam ring of the antibiotics via a hydrolytic mechanism, rendering the antibiotic useless.[18,30-32]

By the year 2009, over 890 unique sequences existed for β-lactamase enzymes.[33,34] To avoid confusion, an organized grouping system was needed that would make indentifying the β-lactamases simple. Based on their primary structure, B-lactamases can be categorized into four classes: A, B, C, and D.[34-37] Class A, C, and D enzymes have serine in their active site and the β-lactam antibiotic is hydrolyzed through formation of acyl-enzyme complex.[33-37] Class B β-lactamases are metalloenzymes; meaning that they require a metallic ion such as Zn in the active site in order for them to carry out hydrolysis of the antibiotic substrate.[33-36]

1.1.3 Carbapenem-hydrolyzing Class D β-Lactamases in *A. baumannii*

The harshest of *A. baumanni* infections were treated with carbapenems, which are the most stable antibiotics towards hydrolysis by β-lactamases.[38] First introduced over 30 years ago,

the carabapenem antibiotics have now become susceptible to hydrolysis by all four classes of β-lactamases.[28,39-41] Carbapenem-resistant *A. baumannii* has emerged worldwide due to their ability to produce carbapenem-hydrolyzing Class D β-lactamases (CHDLs).[28,42-44] Class D β-lactamases are able to hydrolyze the β-lactam antibiotic oxacillin (a penicillin) and are thus are given an alternative title of OXA β-lactamases.[33,37]

Nine total subgroups exist for CHDLs.[39,45-47] The most prominent CHDLs in *A. baumannii* are OXA-23, OXA-24, and OXA-58, which all belong to a different subgroup.[28,29,48] The structure of OXA-24 has been elucidated and the structure shows a hydrophobic cleft over the active site.[49-51] A CHDL from *Klebsiella pneumonia* called OXA-48 has a crystal structure depicting absence of the hydrophobic cleft and that active site has a different shape than that of OXA-24.[52] This suggests that the mechanisms the two enzymes employ for carbapenem hydrolysis are different, arising from minor differences in the active sites.[52]

1.1.4 OXA-58, a CHDL of *A. baumannii*

Carbapenem hydrolyzing class D β-lactamase OXA-58 was identified for the first time in France in 2003.[53] This enzyme is the sole member of a CHDL subgroup, sharing less than 50% sequence identity compared to remaining CHDL subgroups.[39,47]

The homology model presented by Dr. Golemi-Kotra and colleagues sheds light on certain structural elements of OXA-58.[54] Like other serine active site β-lactamases, OXA-58 has conserved catalytic motifs. The motif SXXK (residues 83-86) in the active site is responsible for participating in the hydrolytic reaction with antibiotic.[54] Carbamylated lysine in the active site improves the catalytic efficiency of the enzyme.[54] The hydrophobic residue Phe-113 and Phe-114 lie on α3-α4 loop and and Met-225 lies on the β4-β5 loop.[54] Hydrophobic interactions

between the side chains of these residues is probably the reason why a narrow tunnel like entry into the enzyme's active site is visible in the homology model.[54] The Arg-263 residue interacts with the carboxylic group of β-lactams when they're in the active site.[54]

1.2 Mechanism of β-lactam hydrolysis by OXA-58

Serine-active site β –lactamases like OXA-58 hydrolyze β-lactams in two steps: acylation of the enzyme, and then a deacylation step (figure 1.2).[54] First there is formation of acyl-enzyme species following a nucleophilic attack by the active site serine.[54] At this point, the antibiotic is covalently stuck in the enzyme active site. For the enzyme to be able to carry out its purpose of breaking down more and more antibiotics, it needs to regenerate itself. That's when the second step comes into play. The enzyme is de-acylated via hydrolysis by a water molecule and the active site becomes free to convert more substrate molecules into products.[54]

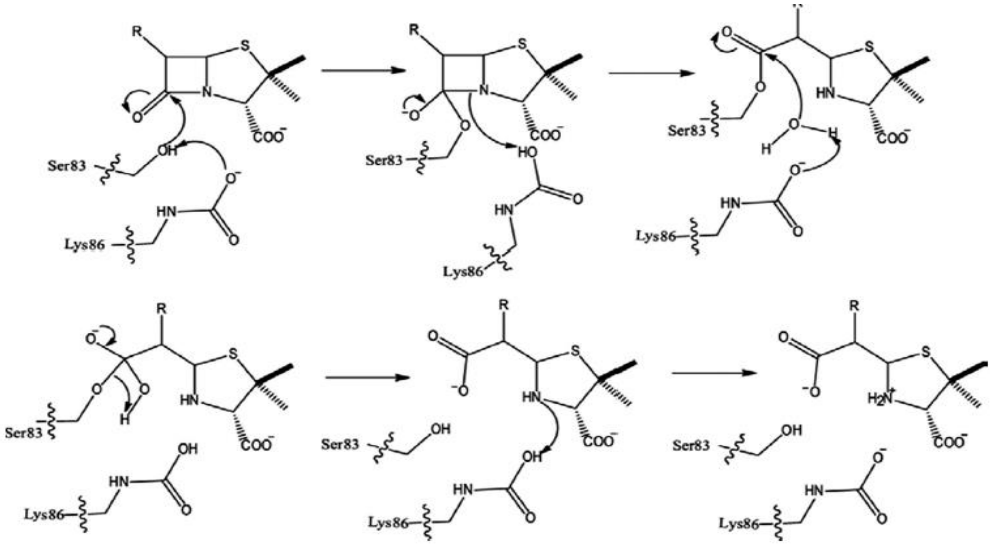

Figure 1.2 Hydrolytic mechanism of OXA-58.[54] The conserved SXXK motif (residues 83-86) in the active site participates in the hydrolytic reaction with antibiotics.[54] The catalytic efficiency is improved when the lysine is carbamylated.[54] It acts as a general base by activating the serine in the first step and water's –OH group in the second step, to carry out nucleophilic attacks.[55,56]

1.3 Isothermal Titration Calorimetry (ITC)

Studying the kinetics of OXA-58's reaction with various substrates is important in order to come up with for novel drug designs for treatment of antibacterial infections. One of the techniques that can be utilized to determine such parameters is Isothermal Titration Calorimetry (ITC). The general concept by which ITC works is by measuring the heat absorbed/released during a chemical reaction between protein-protein, protein-DNA and in our case enzyme-small molecule.[57-59] The heat change over time is plotted against the reaction time to obtain kinetic parameters like the catalytic rate constant (k_{cat}) and Michaelis constant (K_m) from a single experiment.[60,61] From the ratio k_{cat}/K_m, the enzyme's catalytic efficiency can be determined.[60]

ITC has several advantages over other analytical techniques, making it desirable for kinetic parameter measurements. ITC provides a label free approach as there is no need to link the substrate to a fluorescent molecule and the enzyme is not destroyed in the reaction process; also the technique can be used to study substrates that are physiological and synthetic; additionally, ITC is ideal when materials are limited as there is little sample consumption.[60,62-64]

The general instrumental setup is shown in figure 1.3 A, inspired from the figure in Freyer and Lewis (2008).[61] An adiabatic jacket holds two cells; one for reference solution and one for sample.[57,58,61] The reference is supplied with constant power.[57,58,61] Injection of either enzyme or substrate solution, via spinning syringe, into the other initiates the reaction in sample cell.[57,58,61] There is an absorption/release of heat during the reaction, which is detected by a thermopile device.[57,58,61] A signal is sent by feedback circuit to either increase or decrease power supplied to sample cell.[57,58,61] Power is input into the sample cell for endothermic reactions, while for exothermic reactions power supply is reduced, maintaining the temperature difference

between the reference and sample cells at zero.[57,58,61] The type of raw data curve that an exothermic reaction generates is shown in figure 1.3 B.

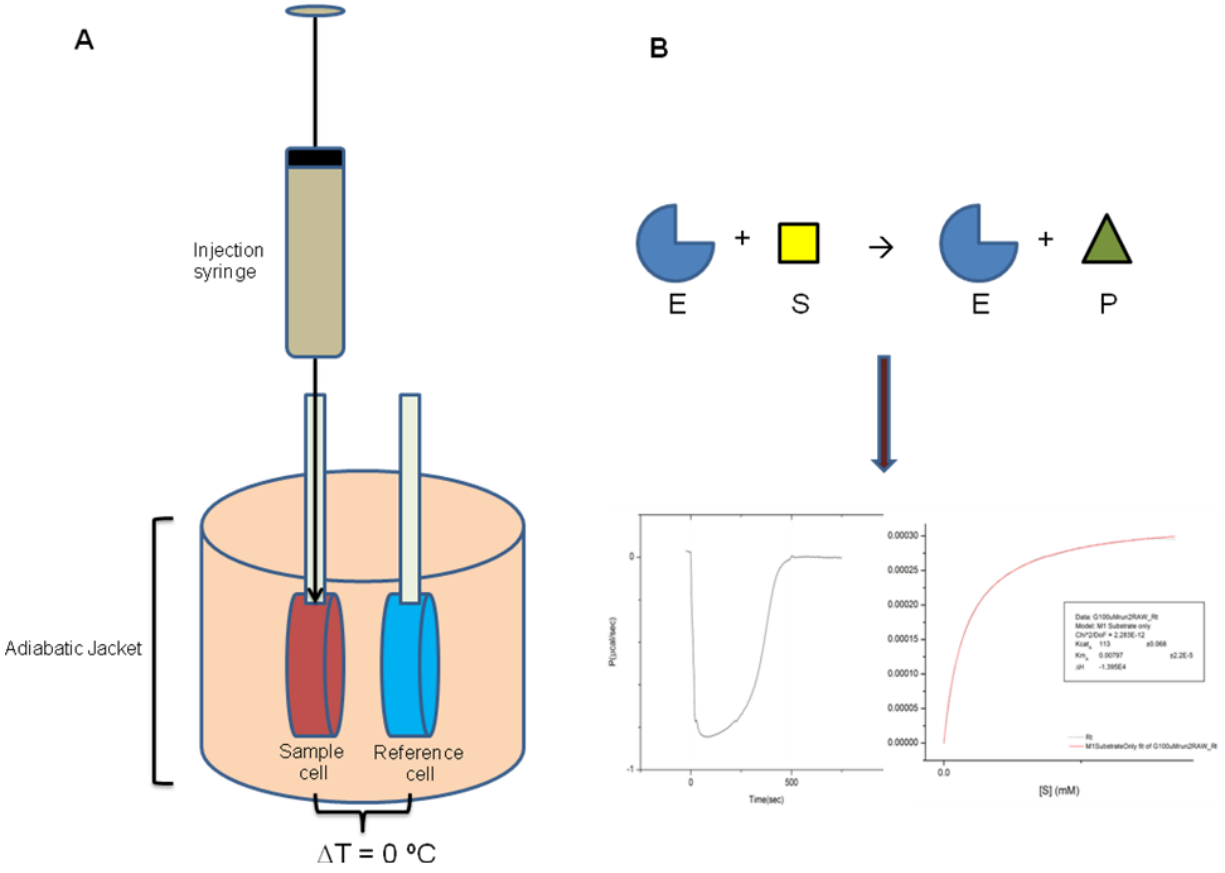

Figure 1.3 A) Schematic of Isothermal titration calorimeter. Injection of protein into the substrate in sample cell initiates the reaction and the absorption or release of heat is detected.[57,58,61] **B) Sample exothermic reaction.** As the substrate is converted into product, the release of heat is offset by the instrument by decreasing power.[57,58,61] Kinetic parameters are obtained directly by fitting the curve. For an endothermic reaction, heat is absorbed and the instrument offsets that change by increasing the power.[57,58,61]

1.4 Hydrogen-deuterium exchange (HDX)

Proteins are important biochemical molecules because they control vital biological processes. Therefore understanding protein structure and dynamics at molecular level is an

important topic in biochemistry and the focus of this dissertation. It is widely known that the structure of a protein gives rise to its function. Popular techniques like X-ray crystallography and Nuclear Magnetic Resonance (NMR) Spectroscopy are routinely employed to study protein structure, which paint a still picture of native protein under physiological conditions.[65,66] Proteins, however, do not always maintain one shape. It is widely recognized that proteins are very dynamic and therefore continuously changing conformations, which is essential for proper functioning.[67,68] From ligand binding to catalysis, proteins are able to carry out their activity due to the fact that they briefly sample conformations higher in energy than the native state.[69-73] These excited states are short-lived and therefore hard to analyze with the aforementioned conventional methods for studying structure.

Time-resolved electrospray ionization mass spectrometry (TRESI-MS) and hydrogen-deuterium exchange (HDX) are used in combination to study such rapid, activity-linked dynamic motions in proteins. The principle of Hydrogen deuterium exchange (HDX) is a simple in terms that it is a reaction where deuterium (D_2O in solution) replaces a labile hydrogen atom of a molecule.[74,75] The analytical technique of mass spectrometry (MS) separates and helps identify analyte ions based on their mass to charge ratios. When H is replaced by the heavier isotope D, it shows up on a mass spectrum as an increase of one unit for every exchange event.

For a protein, hydrogen groups such as –SH, -OH and $-NH_2$ on side chains undergo very fast exchange, making HDX measurements problematic because as soon as the deuterium exchanges for hydrogen, hydrogen re-exchanges for deuterium. The HDX rate is very high at the side chains and is not detected by Mass Spectrometry. For real-time measurements, one must consider only the backbone amide hydrogens.[76] These are known as backbone hydrogens (also

slow exchanging hydrogens) because these hydrogens are present at the peptide linkages (N-H to be specific) that connect all of the amino acid residues together.[76] One can analyze HDX data for these amide hydrogens to get a full picture of the protein's structural and dynamic features since the amide hydrogens are evenly distributed down the length of the protein.[76] The hydrogen at N-terminus of the peptide (from first amino acid) cannot be counted as backbone amide hydrogen because there is no peptide bond at that end.[76] Also, Proline's structure does not have a slow exchanging hydrogen since its side chain loops back on itself to connect with Nitrogen atom.[76]

Information on the protein's secondary and tertiary structures can be obtained from HDX-MS.[74,76] The more structured regions involve a large number of intramolecular hydrogen bonding and experience less solvent accessibility, so there's low level of deuterium uptake. The less structured regions experience less hydrogen bonding and greater solvent accessibility and thus larger deuterium uptake.[76]

HDX in NMR Spectroscopy is measured as volume decrease of backbone amide hydrogens in Heteronuclear Single Quantum Coherence (HSQC) cross-peaks over time.[77] NMR spectroscopy can provide site specific information on protein structure; however it requires a large amount of pure protein in order to monitor its conformational changes.[78-80] Also because the conventional backbone-amide HDX experiments generate data usually measured in the minutes-to-hours time scale, one cannot examine the more dynamic regions possibly associated with functioning/activity of a protein.[76,81,82] In order to monitor these more dynamic protein regions, a novel custom-built microfluidic device was attached to the front end of the mass spectrometer, which allowed acquisitions to be made in the millisecond time scale. In the

microfluidic device the residence time was small; therefore the back-exchange (from D back to H) was minimized.

1.4.1 Top-down and bottom-up approaches for HDX

HDX experiments on proteins using a mass spectrometer can be carried out using two approaches: top-down and bottom-up. In the top-down experiment, deuterated proteins in the gas phase are fragmented.[83] This method can provide resolution up to single-residue using the electron capture/transfer dissociation method.[69] This method prevents scrambling of deuterium position (i.e. random rearrangement of H/D on labile peptide hydrogens), but these dissociation methods require more specialized equipment.[69,84-86] Also, fragmentation efficiency decreases with increasing peptide size, which is another disadvantage of using the top-down method for protein HDX-MS.[69]

In bottom up technique the H/D exchange on a protein is first quenched by an acid and then the protein is digested into peptides by acid-resistant protease.[87] Peptides that are 4-10 residues in length can be identified using this approach, where spatial resolution is directly related to digestion efficiency (more resolved = better digestion profile).[76] Advantages of using bottom-up approach are that it requires no specialized equipment, and there is no size limit for the molecule being investigated. In this study we utilize the bottom-up approach to measure the dynamics of β-lactamase OXA-58.

1.4.2 Continuous vs. Pulse-labeling methods

There are two methods for deuterium incorporation on the proteins: continuous labeling and pulse labeling. Continuous labeling is the method where protein is mixed with deuterated

solvent for different incubation periods and from this, the exchange rate and amount of deuterium uptake are determined. The conformational dynamics the protein exhibits in its native state can be monitored using this setup.[83,88,89] In pulse labeling experiments, the protein is labeled by exposure to a short deuterium pulse (ms), at varying incubation times after start of the reaction.[90,91] This gives a picture of the protein structure at the instant the pulse is applied. For monitoring the dynamics of OXA-58 in this thesis, continuous labeling setup was used.

1.5 Mass Spectrometer – The instrument

Mass Spectrometry (MS) is a powerful analytical technique where the ions are separated based on their mass-to-charge ratio (*m/z*) and their structural, chemical and quantity information is extracted. There are three main components in mass spectrometers: ion source, mass analyzer and ion detector. In this work, ions produced by Electrospray ionization are analyzed by a Quadrupole time-of-flight tandem mass spectrometer.

1.5.1 Electrospray ionization (ESI)

In ESI a high voltage is applied to the solution flowing in a capillary kept at atmospheric pressure, which results in formation of positive and negative ions at the capillary tip.[92,93] ESI in positive ion mode results in accumulation of positive ions at the tip (figure 1.4), which want to get reduced at the curtain plate.[92,93] The shape of a cone known as Taylor cone forms just before small droplets overcome surface tension and break off due to increasing coulombic attraction (figure 1.5).[92,93] These small droplets are eventually converted to gas phase analytes as they travel though air in atmospheric pressure zone.[92,93]

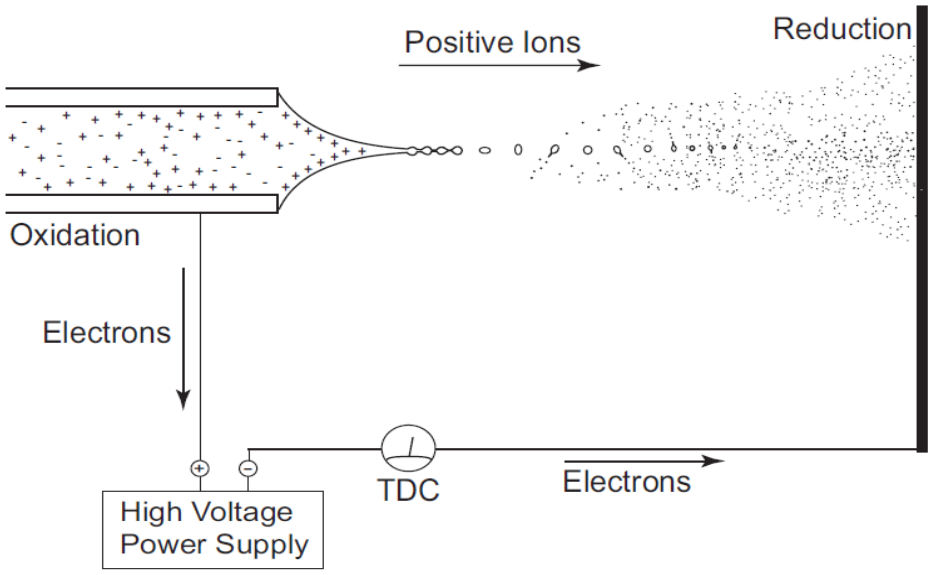

Figure 1.4 Diagram of the electrospray ionization procedure.[92] In the positive ion mode, applying voltage to the capillary results in the positive ions (accumulated at the tip) to fly towards the curtain plate to red reduced.[92,93]

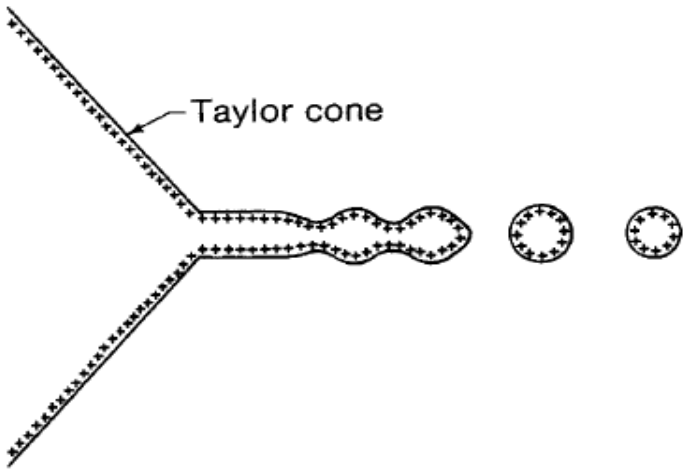

Figure 1.5 Schematic illustration of Taylor cone.[93] The shape of a cone is visible at the capillary tip just before small droplets overcome surface tension and break off due to increasing coulombic attraction.[92,93]

1.5.2 Quadrupole time-of-flight (Q-TOF) mass spectrometer

The setup used for the experiments in this work is that of Quadrupole time-of-flight (Q-TOF) mass analyzer, where a triple quadrupole's third quadrupole Q3 is replaced by a Time-of-flight (TOF) analyzer. This design is ideal for protein characterization studies. Quadrupole QO is present in front of Q1 and Q2 quadrupoles, which is needed for collisional cooling and ion focusing.[94] The Two quadrupoles Q1 and Q2 select/separate ions based on their path in oscillating electric fields.[94] Finally the ions are passed on to TOF where they are separated based on kinetic energy and velocity.[94] Ions are accelerated by a known strength electric field and because they have different mass-to-charge (*m/z*) ratios, they reach the detector at different times. The micro-channel plate (MCP) detector propagates the signal and the final output is displayed on the computer screen as mass spectra.

1.6 Research objectives

The purpose of the research project is to measure the kinetic parameters and enzyme dynamics of the OXA-58 β-lactamase as it turns over various β-lactam antibiotics that vary from one another through side chains.

The catalytic efficiency at which the antibiotics are turned over will shed insights into which side elements of a side chain are most important in terms of reducing the efficiency of the enzyme. Drugs of the future can be generated keeping the "enzyme-hindering" side chain motifs in mind.

The dynamics of the enzyme with different antibiotic substrates provides insights into the regions of enzyme being affected the most and least upon the introduction of the antibiotic in the enzymatic solution. High spatial resolution helps identify specific amino acid sequences of the

enzyme that are affected most/least during the catalytic process. Knowing the mechanism of antibiotic hydrolysis and the motions of the enzyme through the reaction are key to developing β-lactamase resistant antibiotics and inhibitors, to ultimately combat drug resistance.

Chapter 2

Experimental

2.1 Materials for protein purification and ITC experiments

Antibiotics and chemicals were purchased from Fisher (Whitby, ON, CA) or Sigma-Aldrich (Oakville, ON, CA). Growth media was supplied by Fisher. Chromatography columns and media were bought from GE Healthcare (Mississauga, ON, CA).

2.2 Protein purification: OXA-58 and mutants

Cloning of OXA-58 was carried out by a previous member in the Dr. Golemi-Kotra lab. Detailed cloning protocol and purification procedures can be obtained by referring to Verma et al.[54] Briefly, a seed culture of *E. coli* BL21(DE3) with the expression vector was grown at 37 °C overnight in the Luria Bertani (LB) medium having 50 μg/ml kanamycin. A 2.5 mL aliquot of the culture was diluted in 800 mL Terrific Broth (TB) medium containing 50 μg/ml kanamycin. Cells were grown at 37 °C until an optical density was reached in a range of 0.5-0.8 at 600 nm absorbance. Then isopropyl β-D-1-thiogalactopyranoside (IPTG) was added to make a final concentration of 0.1 mM to induce overexpression. The protein was expressed overnight at 25 °C. Cells were pelleted at 6,000 x g for 15 min and then resuspended in 10 mM sodium phosphate buffer, pH 6.4. Cellular contents were released by sonication and the cell debris was pelleted by spinning at 25,000 x g for one hour. The resulting supernatant was loaded onto Sulfopropyl-Sepharose cation exchange column and the protein was eluted in a linear gradient of 10–200 mM sodium phosphate, pH 6.4. Collected protein fractions were concentrated and finally buffer exchanged into 50 mM sodium phosphate buffer, pH 7.0. The purification procedures

were carried out at 4 °C.[54] The concentration was measured using the NanoDrop 2000 UV-Vis Spectrophotometer (Thermo Scientific, Waltham, MA, USA).

A previous lab member generated the OXA-58 mutants, which were stored in the freezer. They were used to carry out the experiments. In the cases where there was need to purify, stored seed cultures of the mutants were used to purify them using the exact same protocol as that for OXA-58 WT.

2.3 Circular dichroism (CD) for determining secondary structure and protein concentration

CD is a spectroscopic technique that is utilized to study chiral molecules and used extensively to determine the secondary structure of macromolecules such as proteins. Jasco J-815 CD spectrometer was used to obtain CD-spectra in the far-UV region for OXA-58 WT and its mutants. Spectral measurements were made at 20°C temperature in 50 mM sodium phosphate buffer, pH 7.0, in a cuvette with a pathlength of 0.1 cm. Measurement range was from 260 to 200 nm, taken at a scan rate of 20 nm/min, with 8 sec response and 1 nm bandwidth. All acquired spectra were adjusted appropriately to correct for buffer contribution.

2.4 Ultraviolet-Visible (UV-Vis) Spectroscopy for OXA-58 kinetics with Nitrocefin

The substrate nitrocefin is a chromogenic cephalosporin that is sensitive to light. So the catalytic parameters (K_m and k_{cat}) of OXA-58 WT and mutants with nitrocefin were determined under steady-state conditions using a Cary 100 Bio UV-visible spectrophotometer (Varian Inc., Palo Alto, USA). Nitrocefin (10–200 μM) was mixed with enzyme (10-40 nM). Molar extinction

coefficient for Nitrocefin is ε486 = 20,500 M^{-1} cm^{-1}. The initial reaction rates were determined at 6% turnover of substrate and the kinetic parameters were measured from the Lineweaver-Burk plots (1/Rate vs. 1/nitrocefin concentration). The reactions were carried out at room temperature in 50 mM Sodium phosphate buffer, pH 7.0.[54]

2.5 Isothermal titration calorimetry for OXA-58 kinetics

Isothermal titration calorimetry (ITC) experiments were carried out using the GE Healthcare instrument MicroCal iTC-200, following the protocol developed by Kotra and colleagues.[95] The measurements were taken at room temperature. The enzyme and antibiotic solutions were prepared in 100 mM sodium phosphate buffer, pH 7.0, supplemented with 50 mM sodium bicarbonate. The antibiotic was kept in the sample cell and the buffer was kept in reference cell. A concentrated OXA-58 solution was in the injection syringe. A single injection of the enzyme into the substrate initiated the reaction, causing a heat change proportionate to the amount of substrate converted to products. That is, the rate of heat flow directly relates to the reaction rate.[60,61] The final concentration of OXA-58 in the sample cell was kept at 1- 600 nM, depending on the injection volume. Analysis of raw data was done using Origin 7.0 software. The raw data produced thermograms that were analyzed in the enzyme assay mode in Origin software after correcting for heat of dilution. Using the Michaelis-Menten equation $Rt = (k_{cat} * E_{tot} * St) / (K_m + St)$, the program computed the kinetic parameters k_{cat} and K_m.[54] Here the substrate concentration (St) is the independent variable and reaction rate (Rt) is the dependant variable; E_{tot} is the enzyme concentration; k_{cat} and K_m are parameters that we are determining.

2.6 Materials for mass spectrometry experiments

Pepsin, deuterium oxide (D_2O), ammonium acetate (≥99.0%), ammonium hydroxide, hydrochloric acid solution, and high purity acetic acid (≥99.7%) were purchased from Sigma-Aldrich. Millipore Milli-Q Advantage A10 Ultrapure Water Purification System was used to obtain high quality water. Small Parts, Inc. (Miramar, FL, USA) supplied metal capillaries (larger: O.D. 400 μm, I.D. 200 μm and smaller: O.D. 318 μm, I.D. 158.75 μm). Polyimide coated glass capillaries (O.D. 153 μm, I.D. 75 μm) were purchased from Polymicro Technologies (Pheonix, AZ, USA). Polytetrafluoroethylene tubings (O.D. 1/16″, I.D. 400 μm and O.D. 1/16″, I.D. 205 μm) were purchased from McMaster Plastics (Scarborough, ON, CA). 1/16″fittings were purchased from Upchurch (Oak Harbor, WA, USA). Silicon rubber was purchased from Rubber Sheet Roll (Shippensburg, PA, USA).

2.7 Microfluidic Device Fabrication

The microfluidic chip is made of a reactangular poly(methyl methacrylate) or PMMA material, on which the channels are etched. Professional Plastics (Fullerton, CA, USA) supplied the PMMA chips. First comes a rapid mixing unit[96] where the protein reacts with deuterium and gets labeled (figure 2.1 A). Then there is the proteolysis chamber[97] where the labeled protein is digested into peptides (figure 2.1 B). A LASER engraver (Universal Laser, Scottsdale, AZ, USA) was used to etch channels on the PMMA chip as described by Rob et al.[96] The rapid mixing device is the orange coloured line in figure 2.1 B and is essentially composed of a smaller glass capillary inside a larger metal capillary. There is a notch cut in the glass capillary 2 mm from the start of capillary. The start of the glass capillary is blocked off by melting the capillary using the Laser engraver. The protein and deuterium solutions mix in the narrow gap between the

inner glass and outer metal capillaries. The second metal capillary to its right is larger in size and through it the low pH acid (pH 2.3) flows that is used to quench the HDX reaction. The solutions are pumped into the microfluidic chip using Harvard Apparatus syringe pumps (Harvard, Holliston, MA, USA) connected to the channels using Polytetrafluoroethylene (PTFE) tubing. The quenched solution makes its way into the proteolytic chamber in the centre of the PMMA chip, which consists of a wet pepsin agarose sitting in an etched out well. A silicon rubber was used to seal the microfluidic setup chip by placing the rubber between two PMMA blocks and clamping the entire assembly tightly using a custom built clamp (LAC Machine & Tooling Limited, ON, CA).[97]

2.8 Continuous labelling Hydrogen-deuterium exchange measurements

HDX measurements were carried out on OXA-58 using the custom built microfluidic chip coupled to the QSTAR Elite hybrid quadrupole time-of-flight mass spectrometer (Sciex, MDS Analytical Technologies, Concord, ON, CA). Experiments were carried out in positive ion mode using ESI source kept at room temperature. 100 µM protein was mixed with D_2O in 1:3 ratio in the rapid mixing unit of the device (figure 2.1 A). Flow rates of protein, D_2O and acid were 2, 6 and 12 µl/min respectively. Labeling time was controlled by adjusting the position of the mixer in the mixing unit, with larger mixing volume translating to an increased labeling. 4% Acetic acid, pH 2.3, was used to quench the labeling. The labeling time ranged from 20 ms to 1.65 s. To minimize the back-exchange, labeled protein digest was shifted to the mass spectrometer in a few seconds, which was quick. Analyst QS 2.0 Software was program used to visualize the mass spectra and from which raw data was extracted.

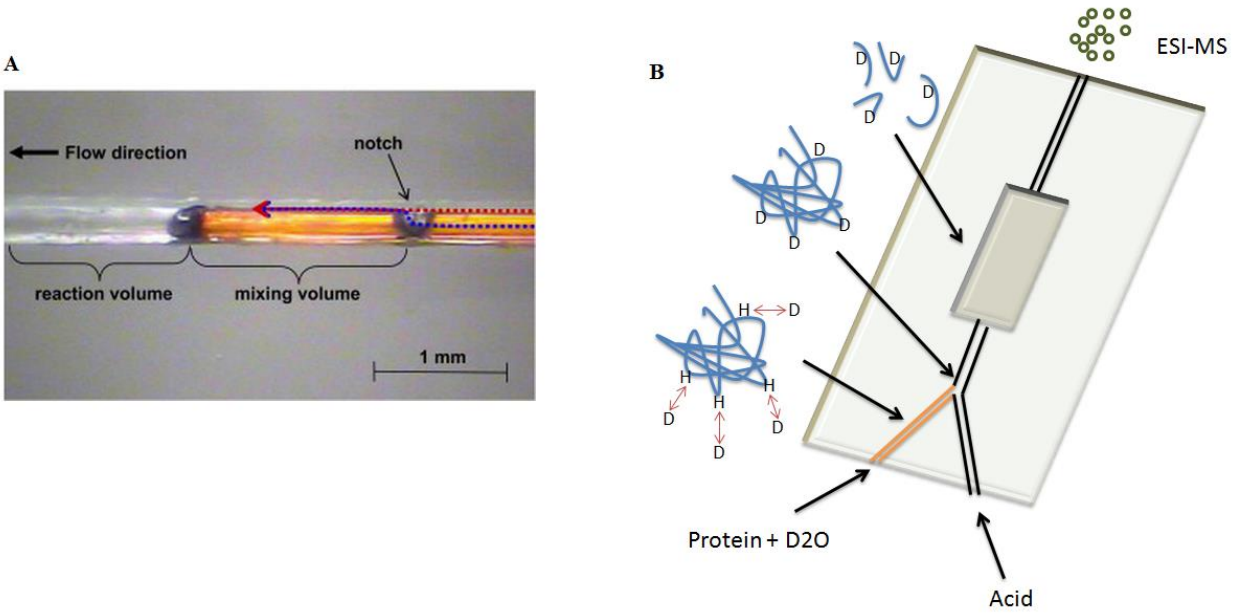

Figure 2.1 A) The adjustable mixer.[96] Protein and D_2O mix in this rapid mixing unit. By pulling back on the golden glass capillary situated inside the metal capillary, the reaction volume increases. This ultimately results in an increased labeling time.[96] **B) Schematic of continuous labelling HDX setup.**[98] D_2O and protein mix in the golden coloured capillary and the reaction is quenched by acid post-labeling. The labeled protein is digested in the rectangular proteolytic chamber in the center of the chip and sprayed into mass spectrometer as peptides.

Raw mass spectrum displays peptide peaks at their respective *m/z* readings. Beginning with spectrum data, first the identity of peptides was determined. To do so, take the M peak readings for the protein digest spectrum were plugged in FindPept tool on the ExPASy website (www.expasy.org). A peptide list was generated that showed the sequence of the amino acids making up the peptide and the location of that peptide in the overall protein sequence.

The level of deuterium uptake for the peptides was obtained using a custom FORTRAN program, whereby the theoretical isotopic distribution is generated for the percent deuterium

exchange that is input into the programming language. Percent deuterium uptake is confirmed by overlapping isotopic distribution observed during experiment and the one predicted by FORTRAN program. The program takes into account that the side chains and protein termini exchange fast and are therefore not used in the calculations.

SigmaPlot 11.0 was the program used to generate the rate curves that also show the final deuterium amplitude. First, deuterium uptake vs. HDX reaction time graphs were created. Then a dynamic fit curve was generated for the plotted data, from which rate was determined. For OXA-58, exponential rise to maximum, single, 2 parameter equation f=a*(1-exp(-b*x)) was used to create the curve. SigmaPlot report generated at the end displays the coefficients, where 'a' is the amplitude of exchange and 'b' is the rate of exchange. This process was repeated for every peptide to be analyzed.

Upon determining the amplitudes and rates of HDX, the next step was to colour the three dimensional protein structure based on these values. Crystal structure of the carbapenemase OXA-58 from *A. baumannii* was determined by Smith et al. [99] and this structure was used as the template throughout this thesis. The PDB file (PDB code 4OH0) was downloaded from Protein Data Bank (www.pdb.org) and opened using The PyMOL Molecular Graphics System (version 1.1r1), which rendered the protein in 3D. Colours were incorporated into the structure by acting on "cartoon" form of the structure.

Chapter 3

Results and Discussion

3.1 OXA-58 purification

Using SP Sepharose cation exchange column and technique of Fast protein liquid chromatography, the protein was purified by creating a linear gradient of 10-200 mM Sodium phosphate buffer, pH 6.4. The protein eluted between 65-85% of 200 mM sodium phosphate buffer, pH 6.4 as the figure 3.1 A shows a single peak. Figure 3.1 B shows a 12.5% gel obtained using sodium dodecyl sulfate-polyacrylamide gel electrophoresis (SDS-PAGE). Both the chromatogram and the gel indicate that protein was highly pure. The molecular weight of OXA-58 is approximately 29 kDa.

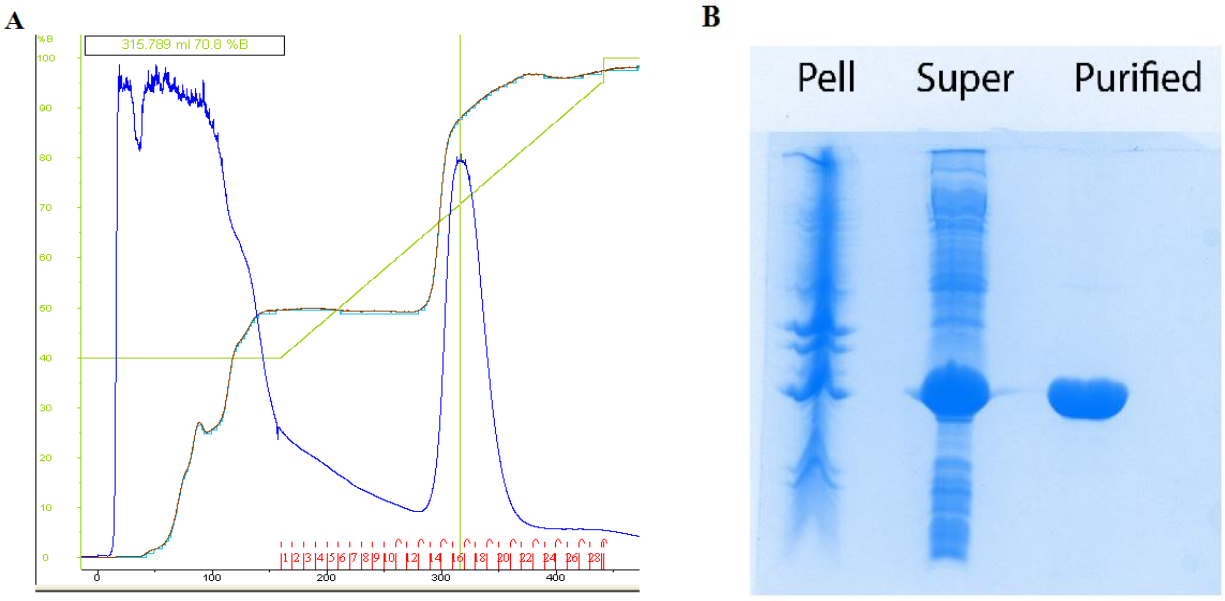

Figure 3.1 A) FPLC chromatogram for OXA-58 purification. The protein eluted at 65-85% of 200 mM sodium phosphate buffer, pH 6.4. **B) 12.5% SDS-PAGE gel for protein identification.** A single dark band indicates there were no degradation products or impurities.

The molecular weight of OXA-58 was confirmed through mass spectrometry. Figure 3.2 A indicates that three main charge states were visible (+11, +10 and +9). Molecular weight can be obtained directly from any of these peaks.

For example, for +10 charge state: [Protein mass + 10 Hydrogens] / 10 = 2896.4728

Protein mass = (2896.4728 x 10) – 10 = 28955 Da ≈ 29 kDa

There appeared to be an adduct of 80 Da attached to the protein (figure 3.2 B), which probably came from a chemical impurity introduced in the buffers during purification procedure. This adduct is believed to be SO_3 as it has a molecular wight of 80 Da. The future experiments were not affected by the presence of this adduct.

A

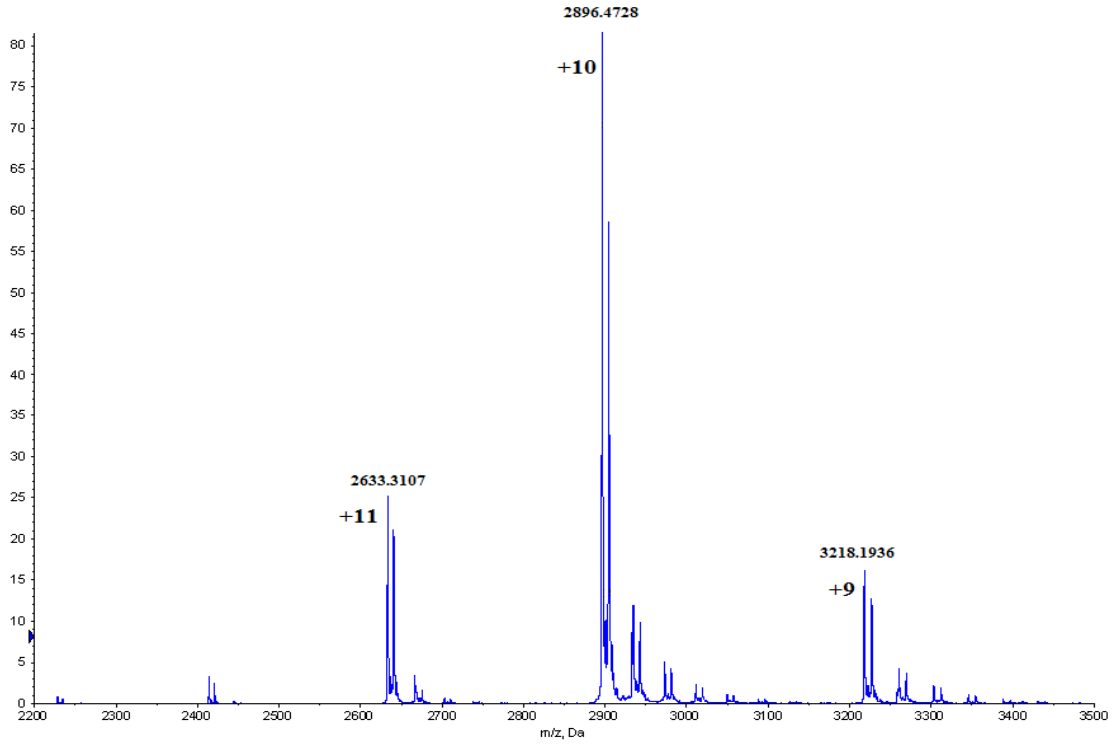

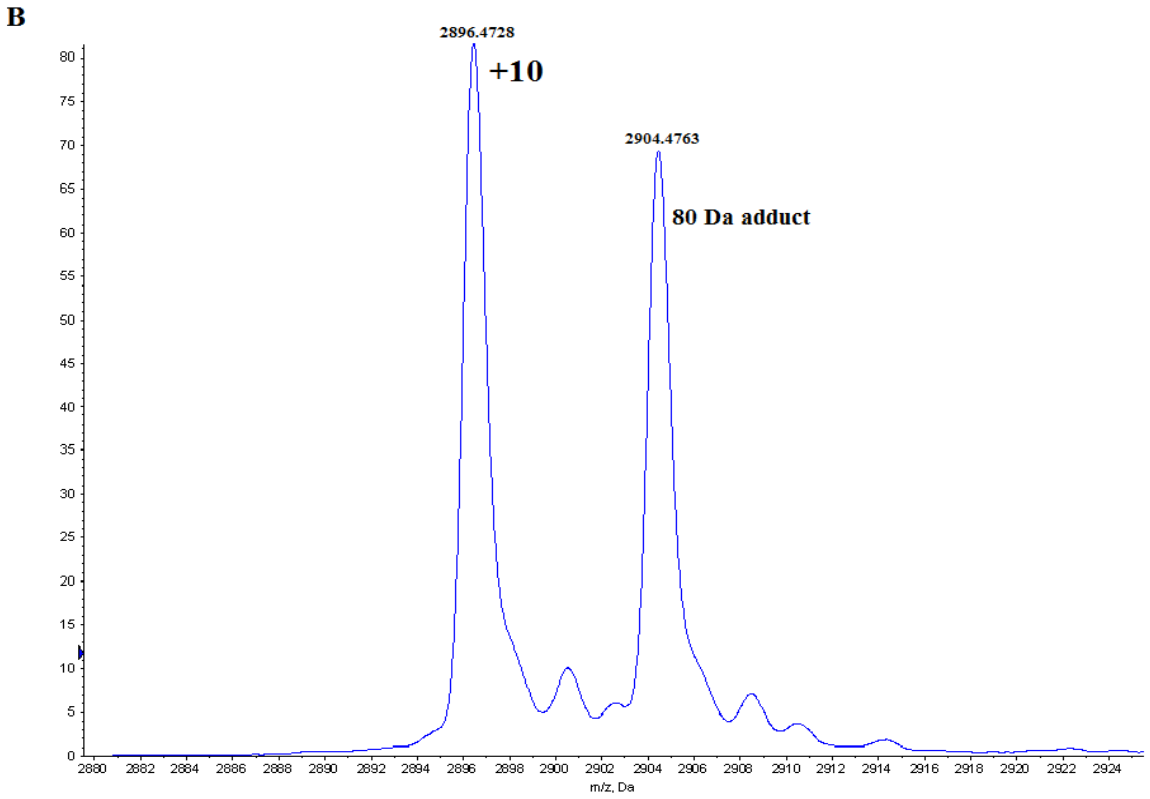

Figure 3.2 A) Mass spectrum for OXA-58. Three dominant charge states are observed, with +10 being the most intense. **B) OXA-58 peak for +10 charge state.** There is an 80 Da mass group attached to the protein and is observed for all charge states.

3.2 CD spectra analysis for concentration determination

The concentrations of WT and mutant enzymes were measured separately using NanoDrop 2000 UV-Vis Spectrophotometer at absorbance of 280 nm. Because the WT protein was most recently purified, its CD spectrum was used a standard to which all the other mutants' spectra were made to overlap. This overlap was achieved after applying a concentration multiplication factor (figure 3.3 A, B). The multiplication factor suggests that the measured concentrations of the mutants using the NanoDrop 2000 UV-Vis Spectrophotometer should

actually be adjusted according to their respective factors to correctly determine their concentrations.

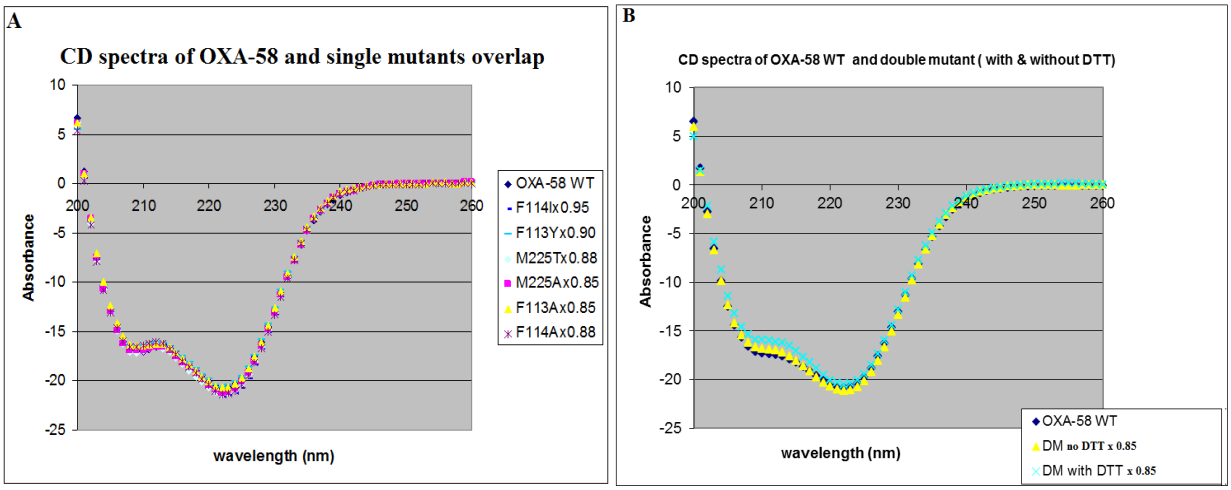

Figure 3.3 A) CD spectra for single mutants of OXA-58. Overlapping the mutants' spectra with that of wild-type enzyme allowed determining accurate concentrations. **B) CD spectra for double mutants of OXA-58.** Accurate enzyme concentrations were determined by overlapping the double mutants' spectra with that of the wild-type OXA-58.

3.3 Measuring OXA-58 kinetics parameters using ITC

The hydrophobic side chains of amino acids Met-225, Phe-113 and Phe-114 extend towards each other (figure 3.4).[54] PDB structure with code 4OH0 was used as the template.[99] Phe-114 and Met-225 lie on two separate loops.[54] Therefore, these residues were mutated individually to generate 6 different mutants and the kinetics of which were compared with the wild-type enzyme using isothermal titration calorimetry. A double mutant (DM) was generated by mutating residues Phe-114 and Met-225 to cysteines. By mutating these residues, the enzyme was cross-linked and this restricted the movement of the enzyme. Kinetics parameters were measured for this double mutant with and without addition of Dithiothreitol (DTT). Hypothesis

is that adding DTT will break the cross-link and make enzyme more flexible to carry out its catalytic activity. The kinetic parameters k_{cat} and K_m obtained for all the mutants are recorded in tables 3.1 and 3.2.

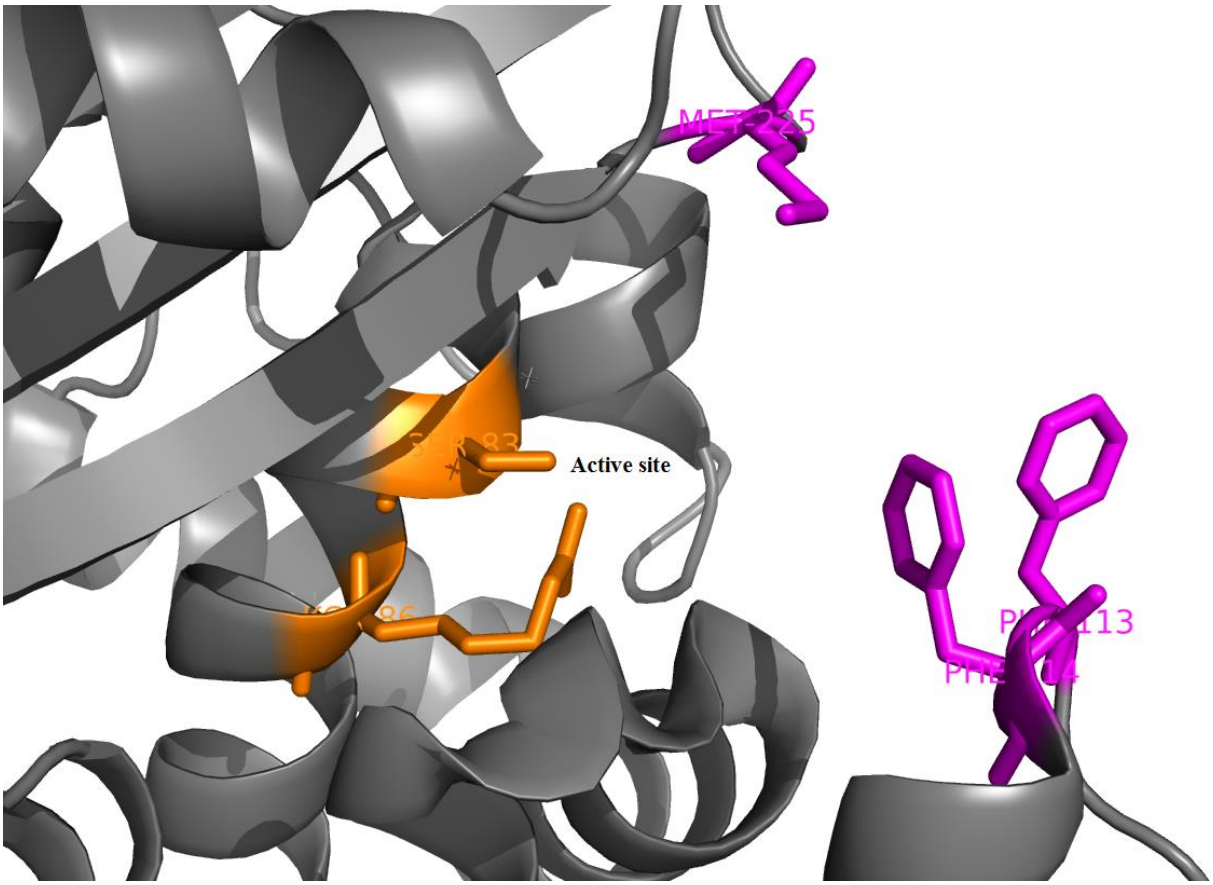

Figure 3.4 Depiction of OXA-58 active site.[99] Side chains of M-225, F-113 and F-114 (magenta) extend towards each other forming hydrophobic interactions.[54] The active site of OXA-58 has the catalytic SXXK motif (orange) spanning across residues 83-86.[54]

Table 3.1 Kinetic parameters for OXA-58 WT and the double mutants

		Penicillin G	Ampicillin	Carbenicillin	Amoxicillin	Oxacillin	Imipenem
WT	**Kcat/Km (s^{-1} μM^{-1})**	**15 ± 3**	**4.6 ± 0.9**	**1.7 ± 0.4**	**2.8 ± 0.5**	**3.5 ± 0.4**	**0.5 ± 0.2**
	k_{cat} (s^{-1})	106 ± 10	97 ± 14	272 ± 13	62 ± 10	137 ± 14	1.2 ± 0.2
	K_m (μM)	7 ± 1	21 ± 3	160 ± 40	22 ± 2	39 ± 3	2.3 ± 0.5
Double mutant F114C-M225C (no DTT)	**Kcat/Km (s^{-1} μM^{-1})**	**1.3 ± 0.1**	**0.13 ± 0.02**	**0.048 ± 0.009**	**0.28 ± 0.05**	**0.04 ± 0.01**	**No reaction**
	k_{cat} (s^{-1})	147 ± 8	70.3 ± 0.4	14 ± 3	121 ± 19	21 ± 6	No reaction
	K_m (μM)	112 ± 11	551 ± 86	291 ± 11	432 ± 38	520 ± 18	No reaction
Double mutant F114C-M225C (with DTT)	**Kcat/Km (s^{-1} μM^{-1})**	**12 ± 2**	**2.6 ± 0.3**	**0.075 ± 0.003**	**1.6 ± 0.2**	**0.13 ± 0.01**	**---**
	k_{cat} (s^{-1})	275± 30	220 ± 17	42 ± 0	288 ± 31	64 ± 2	---
	K_m (μM)	23 ± 2	85 ± 6	562 ± 26	177 ± 16	499 ± 44	---

Table 3.2 Kinetic parameters for OXA-58 WT and the single mutants

		WT	M225A	F113Y	F114A	F113A	M225T	F114I
Penicillin G	**Kcat/Km (s^{-1} μM^{-1})**	**15 ± 3**	**19 ± 4**	**20 ± 2**	**7 ± 1**	**4 ± 1**	**4.1 ± 0.5**	**0.58 ± 0.06**
	k_{cat} (s^{-1})	106 ± 10	141 ± 29	137 ± 9	124 ± 8	37 ± 7	42 ± 3	5.7 ± 0.5
	K_m (μM)	7 ± 1	7.3 ± 0.7	6.9 ± 0.7	17 ± 2	10.3 ± 2.9	10 ± 1	9.7 ± 0.2
Ampicillin	**Kcat/Km (s^{-1} μM^{-1})**	**4.6 ± 0.9**	**1.6 ± 0.3**	**1.6 ± 0.3**	**1.5 ± 0.4**	**0.83 ± 0.09**	**0.52 ± 0.08**	**0.13 ± 0.02**
	k_{cat} (s^{-1})	97 ± 14	75 ± 8	108 ± 4	188 ± 25	39 ± 1	38 ± 4	6.80 ± 0.03
	K_m (μM)	21 ± 3	46 ± 9	66 ± 11	127 ± 25	48 ± 5	72 ± 9	54 ± 9
Carbenicillin	**Kcat/Km (s^{-1} μM^{-1})**	**1.7 ± 0.4**	**3.3 ± 0.5**	**1.1 ± 0.3**	**0.6 ± 0.3**	**0.31 ± 0.05**	**0.25 ± 0.07**	**0.06 ± 0.02**
	k_{cat} (s^{-1})	272 ± 13	102 ± 15	167 ± 15	173 ± 64	44 ± 4	41 ± 4	14.8 ± 0.7
	K_m (μM)	160 ± 40	31 ± 2	153 ± 47	268 ± 65	142 ± 16	161 ± 39	248 ± 66
Amoxicillin	**Kcat/Km (s^{-1} μM^{-1})**	**2.8 ± 0.5**	**3.5 ± 0.7**	**2.9 ± 0.8**	**1.4 ± 0.1**	**0.61 ± 0.04**	**0.7 ± 0.1**	**0.10 ± 0.02**
	k_{cat} (s^{-1})	62 ± 10	97 ± 15	79 ± 7	204 ± 14	24 ± 1	32 ± 4	8.2 ± 0.7
	K_m (μM)	22 ± 2	28 ± 4	27 ± 7	145 ± 5	40 ± 2	49 ± 4	80 ± 10

Oxacillin	**Kcat/Km (s^{-1} μM^{-1})**	**3.5 ± 0.4**	**3.2 ± 0.4**	**1.1 ± 0.3**	**0.05 ± 0.02**	**0.11 ± 0.02**	**0.036 ± 0.005**	**0.0110 ± 0.0002**
	k_{cat} (s^{-1})	137 ± 14	179 ± 14	85 ± 6	59 ± 19	17 ± 3	17 ± 2	3.69 ± 0.04
	K_m (μM)	39 ± 3	56 ± 4	74 ± 21	1.4 ± 0.5 (mM)	156 ± 1	462 ± 24	335 ± 6
Nitrocefin	**Kcat/Km (s^{-1} μM^{-1})**	**4.2 ± 0.3**	**3.8 ± 0.1**	**5.4 ± 0.5**	**0.17 ± 0.04**	**1.5 ± 0.1**	**2.4 ± 0.6**	**0.23 ± 0.07**
	k_{cat} (s^{-1})	95 ± 3	73 ± 1	107 ± 1	28 ± 3	17 ± 1	37 ± 1	3.9 ± 0.7
	K_m (μM)	23 ± 1	19 ± 1	20 ± 2	164 ± 33	11 ± 1	15 ± 3	17 ± 4
Imipenem	**Kcat/Km (s^{-1} μM^{-1})**	**0.5 ± 0.2**	**0.52 ± 0.09**	**0.48 ± 0.08**	**0.10 ± 0.03**	**0.09 ± 0.02**	**0.090 ± 0.007**	**0.011 ± 0.001**
	k_{cat} (s^{-1})	1.2 ± 0.2	0.63 ± 0.02	0.9 ± 0.1	0.442 ± 0.008	0.108 ± 0.008	0.19 ± 0	0.024 ± 0.001
	K_m (μM)	2.3 ± 0.5	1.2 ± 0.2	2.0 ± 0.2	4 ± 1	1.1 ± 0.2	2.1 ± 0.2	2.2 ± 0.2

From figure 3.5 A histogram it is observed that F113A, M225T and F114I have lower turnover rates compared to other mutants. Also, adding 3 mM dithiothreitol (DTT) to double mutant (DM with DTT) tends to increase the turnover rate compared to when no DTT is added (DM no DTT). This is most likely because the enzyme is more flexible to carry out its catalytic activity when the cross-link is broken and so the substrate in the active site is turned over faster. It was noted that most substrates are turned over quicker by the wild-type enzyme than the double mutant with DTT, but amoxicillin and penicillin G are turned over faster by the double mutant with DTT. This was interesting because it indicates that for these two substrates when DTT is added, the protein is more flexible and more catalytically active. This makes sense because there would be no hydrophobic interactions (like in WT) happening between the loops that guide entry of substrates into active site since the cross-link between two cysteines (F114C-M225C) is broken.

Figure 3.5 B indicates that F113A, M225T, F114I, double mutant with and without DTT have weaker binding affinity (higher Km) compared to other mutants. OXA-58 WT, M225A and F113Y have strong binding affinity for all antibiotics. Also, upon comparing double mutant with and without DTT, it was noticed that adding DTT generally increases binding affinity.

The general trend observed from figure 3.5 C is that OXA-58 WT, M225A and F113Y are most catalytically efficient enzymes, followed by double mutant in DTT. The least catalytically efficient mutant is F114I, followed by double mutant with no DTT.

The kinetics of nitrocefin were tested with UV-Vis spectrophotometer to compare different techniques for measuring kinetic parameters. The trend observed for nitrocefin matched that of

other substrates, whose kinetics parameters were obtained using ITC. So the data obtained from all the kinetics experiment is reliable and consistent between different instruments.

Particularly interesting finding was that mutating the phenylalanine-114 side chain to isoleucine hampers the catalytic activity of the enzyme, which means a lot more of F114I mutant is needed for it to be as efficient as the wild-type. This was true for F114I's reaction with every substrate. Phenylalanine side chain is planar compared to that of isoleucine, which has a more branched side chain. Replacing the planar side chain residue with a branched one leads to decreased substrate binding and thus decreased catalytic efficiency of F114I mutant.

The wild-type and single mutants of OXA-58 are very inefficient when it comes to turning over imipenem. The double mutant of OXA-58 doesn't show any activity at all for imipenem, indicating that cross-linking the protein by F114C-M225C linkage severely hampers the catalytic efficiency of the protein.

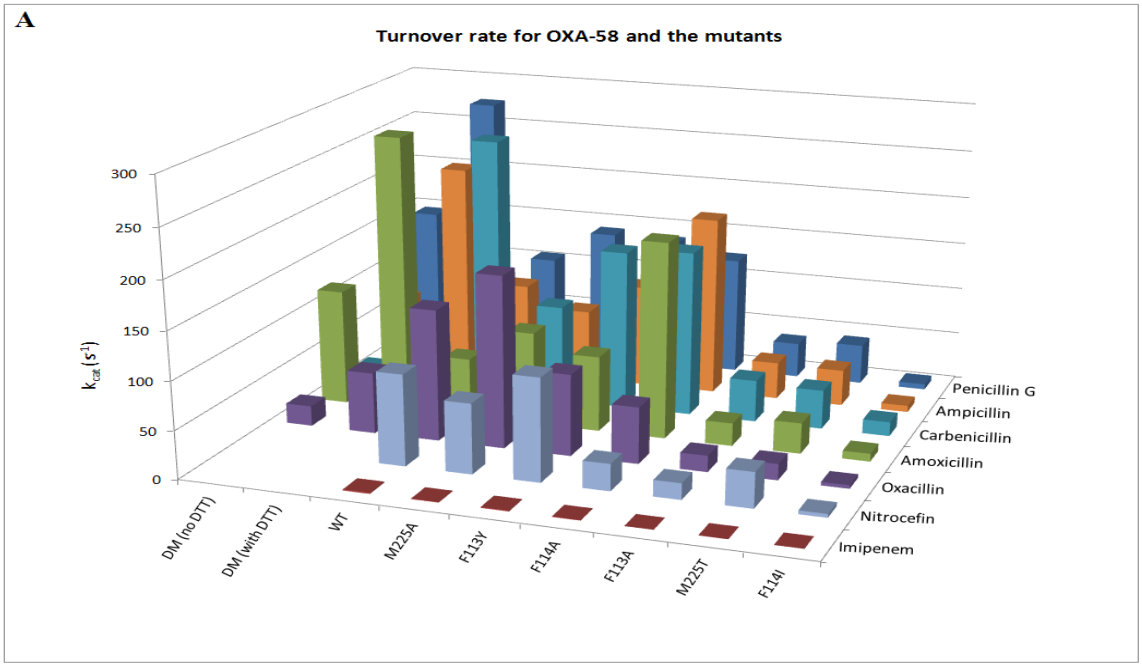

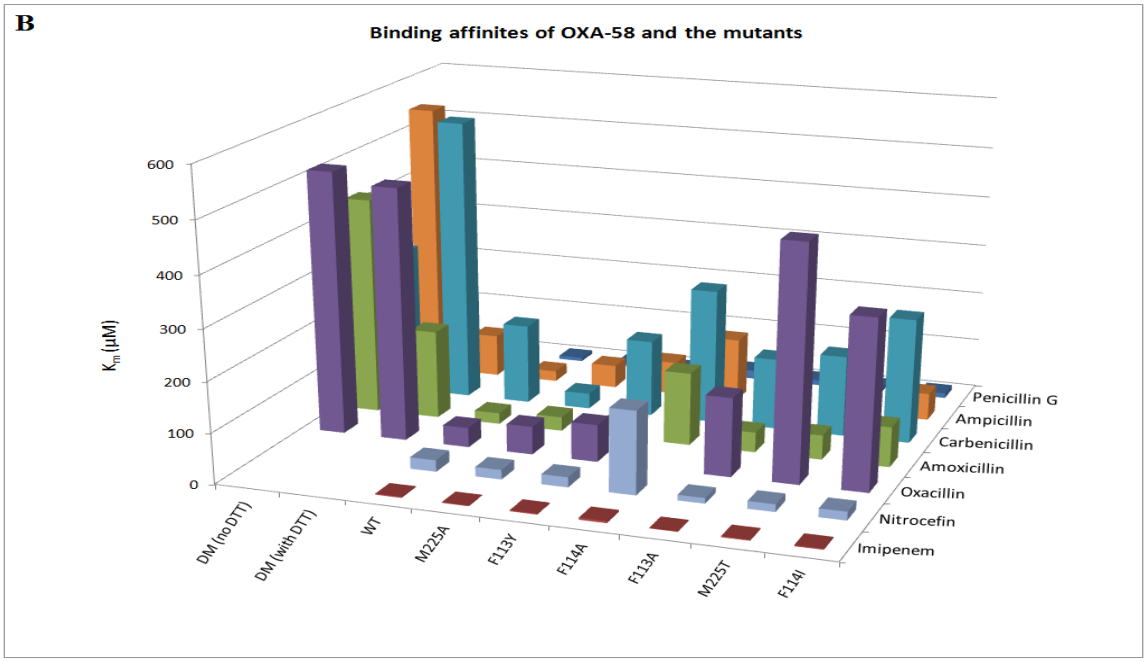

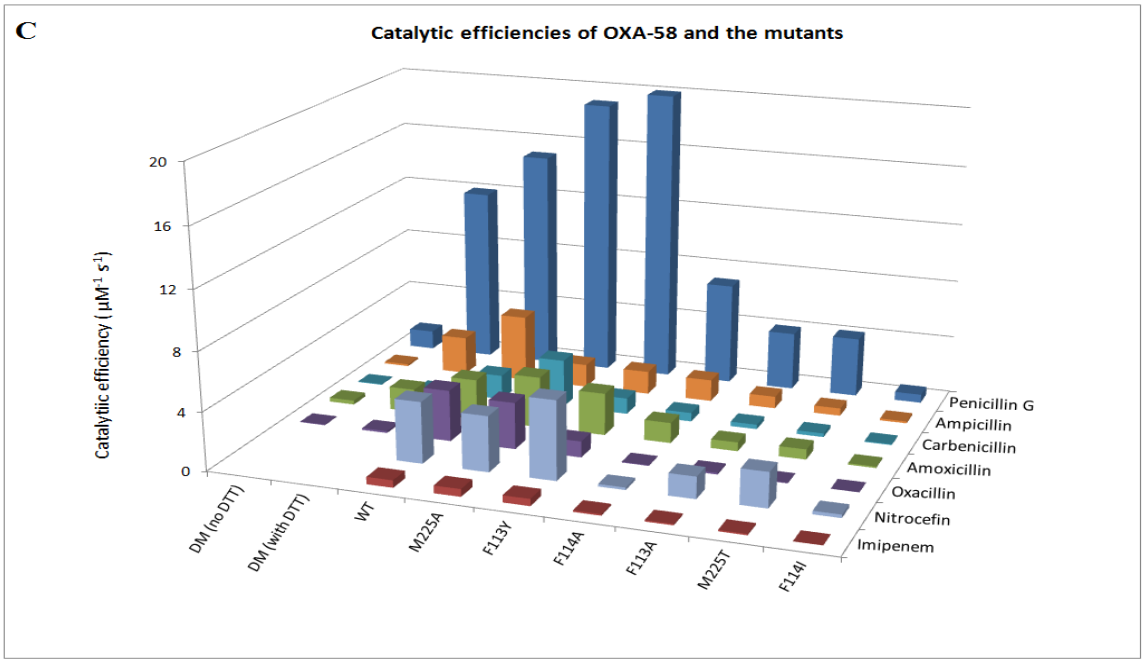

Figure 3.5 3D histograms comparing mutants with OXA-58 WTfor A) turnover rates B) binding affinities and C) catalytic efficiencies. Double mutants (no DTT and with DTT) are positioned on the left of wild-type enzyme and the single mutants are located on the right side. The trend observed is that for all substrates OXA-58 WT and M225A mutant were most catalytically efficient, while F114I mutant was the least efficeint.

3.4 OXA-58 dynamics measured using Mass Spectrometry

The dynamics of OXA-58 were measured in its resting state and its catalytically active state as it reacted with good substrate oxacillin and poor substrate imipenem. Interactions between any enzyme and substrate are typically associated with conformational change in the enzyme. This phenomenon can be described using two models. The conformational selection model is where the substrate selects a specific conformation of the fluctuating substrate-free enzyme, which is most suitable for binding and catalysis. The enzyme displays the same resting state and active state dynamics in this case.[73,100-104] In the induced fit model, the binding of substrate to the resting state enzyme induces a conformational change. This causes catalytically active enzyme to display dynamics that are different from resting state substrate-free dynamics.[105,106]

Tables 3.3, 3.4 and 3.5 show the percent deuterium uptake for the free enzyme OXA-58, good substrate oxacillin-OXA-58 and poor substrate imipenem-OXA-58 reactions respectively. Free enzyme and enzyme-oxacillin experiments were run in triplicates, while enzyme-imipenem experiments were run in duplicate. HDX kinetic plots showing percent deuterium uptake with time were generated for the 12 peptides that were found common in the three experiments (figure 3.6), covering 65% sequence. Four additional peptides were obtained for enzyme-oxacillin and enzyme-imipenem runs (figure 3.7), which increased the sequence coverage to 70%. From the deuterium uptake tables it is evident that there are certain time points that don't have any standard deviation (±) value beside them. This is because these peptides were observed only once, even after repeating the experiments. In those cases, that value was assumed accurate if it fit the trend where the curves rise to maximum in the kinetic plots.

Table 3.3 Percent deuterium uptake for OXA-58

OXA-58

					Deuterium uptake (%)					
m/z	**z**	**M**	**Sequence**	**Location**	**0 ms**	**20 ms**	**170 ms**	**320 ms**	**610 ms**	**1.65 s**
455.26	2	908.51	KAWDKDF	115-121	0	2.67 ± 0	3.11 ± 0.77	4.44 ± 3.08	8.44 ± 3.36	15.10 ± 2.78
469.76	2	937.51	RIGYGNMQ	153-160	0	3.56 ± 0.77	4.00 ± 1.33	4.00 ± 2.31	5.78 ± 2.78	5.33 ± 0
500.83	2	999.64	ARRIGPSLM	139-147	0	2.67 ± 0	4.89 ± 1.54	8.44 ± 0.77	9.33 ± 2.67	22.20 ± 0.77
521.38	2	1040.7	KIANALIGLE	86-95	0	2.67 ± 0	3.56 ± 0.77	6.67 ± 0	7.11 ± 0.77	10.20 ± 2.78
546.34	2	1090.7	DKLGVFHYL	272-280	0	3.11 ± 0.77	4.00 ± 1.33	5.78 ± 0.77	8.44 ± 0.77	16.00 ± 0
581.85	2	1161.7	VEKADGQVVAF	238-248	0	2.67 ± 0	2.67 ± 0	3.11 ± 0.77	4.00 ± 0.77	9.33 ± 0
603.17	5	3010.8	ISADAVFVTYDGQNIKKYGT HLDRAKT	51-77	0	4.00 ± 0	5.33 ± 0	10.20 ± 0.77	20.40 ± 0.77	22.70 ± 0
644.4	4	2573.6	IGLENHKATSTEIFKWDGKP RF	92-113	0	2.67 ± 0	3.56 ± 1.54	7.56 ± 2.04	10.70 ±1.33	18.20 ±1.54
681.76	3	2042.2	ASRAKTSTIPQVNNSIIDQ	24-42	0	4.00 ± 1.89	10.00 ± 4.71	20.00 ± 1.89	28.70 ± 0.94	35.30 ± 0.94
733.91	2	1465.8	TLGEAMQASTVPVY	122-135	0	2.67 ± 0	3.11 ± 0.77	6.67 ± 2.31	7.56 ± 3.36	10.20 ± 1.54
748.48	2	1494.9	WLKGPLTITPIQE	169-181	0	3.11 ± 0.77	3.11 ± 0.77	5.78 ± 1.54	4.89 ± 1.54	9.33 ± 0
896.88	3	2687.6	VYDLAQGQLPFKPEVQQQVK EML	185-207	0	2.67 ± 0	3.11 ± 0.77	6.22 ±1.54	7.11 ± 0.77	11.60 ± 0.77

Table 3.4 Percent deuterium uptake for OXA-58-oxacillin reaction

OXA-58 + Oxacillin

					Deuterium uptake (%)					
m/z	**z**	**M**	**Sequence**	**Location**	**0 ms**	**20 ms**	**170 ms**	**320 ms**	**610 ms**	**1.65 s**
455.26	2	908.51	KAWDKDF	115-121	0	2.67 ± 0	5.33 ± 3.77	7.56 ± 2.78	5.33 ± 0	8.00 ± 0
469.76	2	937.51	RIGYGNMQ	153-160	0	3.56 ± 1.54	4.67 ± 0.94	6.67 ± 1.33	6.67 ± 0	5.33 ± 0
491.85	2	981.67	LARRIGPSL	138-146	0	4.67 ± 0.94	8.00 ± 0	6.67 ± 2.31	10.70 ± 2.31	10.70 ± 1.89
500.83	2	999.64	ARRIGPSLM	139-147	0	4.00 ± 0	8.00 ± 1.89	11.10 ± 0.77	9.78 ± 1.54	12.00 ± 0
521.38	2	1040.7	KIANALIGLE	86-95	0	4.00 ± 1.33	6.00 ± 2.83	5.33 ± 0	7.11 ± 0.77	8.00 ± 0
546.34	2	1090.7	DKLGVFHYL	272-280	0	2.67 ± 0	8.00 ± 0	8.00 ± 0	7.11 ± 0.77	8.00 ± 0
557.37	2	1112.7	LARRIGPSLM	138-147	0	3.11 ± 0.77	6.00 ± 2.83	8.00 ± 0	8.00 ± 0	11.30 ± 0.94
581.85	2	1161.7	VEKADGQVVAF	238-248	0	2.67 ± 0	4.00 ± 0	4.00 ± 0	4.44 ± 0.77	6.67 ± 0
603.17	5	3010.8	ISADAVFVTYDGQNIKKYGT HLDRAKT	51-77	0	5.33 ± 0	13.30 ± 3.77	16.00 ± 2.67	16.00 ± 0	16.00 ± 0
644.4	4	2573.6	IGLENHKATSTEIFKWDGKP RF	92-113	0	4.00 ± 0	7.33 ± 4.71	9.78 ± 2.04	9.33 ± 0	10.70 ± 0
681.76	3	2042.2	ASRAKTSTIPQVNNSIIDQ	24-42	0	6.67 ± 0	28	28.40 ± 5.05	25.30 ± 7.54	26.00 ± 2.83
733.91	2	1465.8	TLGEAMQASTVPVY	122-135	0	2.67 ± 0	5.33 ± 1.89	8.00 ± 2.31	6.22 ± 0.77	8.67 ± 0.94
748.48	2	1494.9	WLKGPLTITPIQE	169-181	0	4.00 ± 0	4.00 ± 0	4.00 ± 0	4.00 ± 0	4.00 ± 0
871.5	1	870.5	AVDPQVGW	226-233	0	2.67 ± 0	4.00 ± 1.89	4.67 ± 0.94	5.33 ± 0	5.33 ± 0
896.88	3	2687.6	VYDLAQGQLPFKPEVQQQVK EML	185-207	0	4.00 ± 0	6.00 ± 0.94	6.67 ± 0	7.11 ± 1.54	8.67 ± 0.94
1035.6	1	1034.6	STVPVYQEL	130-138	0	7.56 ± 0.77	11.30 ± 0.94	11.60 ± 0.77	14.00 ± 2.83	12.70 ± 0.94

Table 3.5 Percent deuterium uptake for OXA-58-imipenem reaction

OXA-58 + Imipenem

					Deuterium uptake (%)				
m/z	**z**	**M**	**Sequence**	**Location**	**0 ms**	**20 ms**	**170 ms**	**320 ms**	**610 ms**	**1.65 s**
455.26	2	908.51	KAWDKDF	115-121	0	2.67 ± 0	2.67 ± 0	5.33 ± 0	8.00 ± 1.89	8.67 ± 2.83
469.76	2	937.51	RIGYGNMQ	153-160	0	2.67 ± 0	2.67 ± 0	4.00 ± 0	5.33 ± 1.89	5.33 ± 0
491.85	2	981.67	LARRIGPSL	138-146	0	2.67 ± 0	2.67	5.33	9.33 ± 1.89	13.30 ± 1.89
500.83	2	999.64	ARRIGPSLM	139-147	0	2.67 ± 0	4.00 ± 1.89	7.33 ± 0.94	10.70 ± 0	14.00 ± 2.83
521.38	2	1040.7	KIANALIGLE	86-95	0	2.67	2.67	4	5.33 ± 1.89	9.33 ± 0
546.34	2	1090.7	DKLGVFHYL	272-280	0	2.67 ± 0	2.67 ± 0	5.33 ± 0	5.33 ± 0	5.33 ± 0
557.37	2	1112.7	LARRIGPSLM	138-147	0	2.67 ± 0	2.67	5.33	8.67 ± 2.83	10.00 ± 0.94
581.85	2	1161.7	VEKADGQVVAF	238-248	0	2.67 ± 0	2.67 ± 0	3.33 ± 0.94	4.00 ± 0	7.33 ± 0.94
603.17	5	3010.8	ISADAVFVTYDGQNIKKYGT HLDRAKT	51-77	0	4.00 ± 0	7.33 ± 0.94	12.70 ± 0.94	16.00 ± 0	16.00 ± 0
644.4	4	2573.6	IGLENHKATSTEIFKWDGKP RF	92-113	0	2.67 ± 0	3.33 ± 0.94	5.33 ± 1.89	8.67 ± 0.94	10.00 ± 0.94
681.76	3	2042.2	ASRAKTSTIPQVNNSIIDQ	24-42	0	2.67	2.67	13.30 ± 3.77	20.00 ± 3.77	17.3
733.91	2	1465.8	TLGEAMQASTVPVY	122-135	0	2.67 ± 0	4.00 ± 1.89	6.00 ± 0.94	8.00 ± 1.89	10.70 ± 1.89
748.48	2	1494.9	WLKGPLTITPIQE	169-181	0	3.33 ± 0.94	3.33 ± 0.94	4.00 ± 1.89	2.67 ± 0	4.00 ± 0
871.5	1	870.5	AVDPQVGW	226-233	0	2.67 ± 0	3.33 ± 0.94	4.00 ± 0	8.00 ± 0	8.00 ± 0
896.88	3	2687.6	VYDLAQGQLPFKPEVQQQVK EML	185-207	0	2.67 ± 0	2.67 ± 0	3.33 ± 0.94	4.67 ± 0.94	5.33 ± 0
1035.6	1	1034.6	STVPVYQEL	130-138	0	2.67 ± 0	5.33	8	9.33 ± 1.89	11.30 ± 2.83

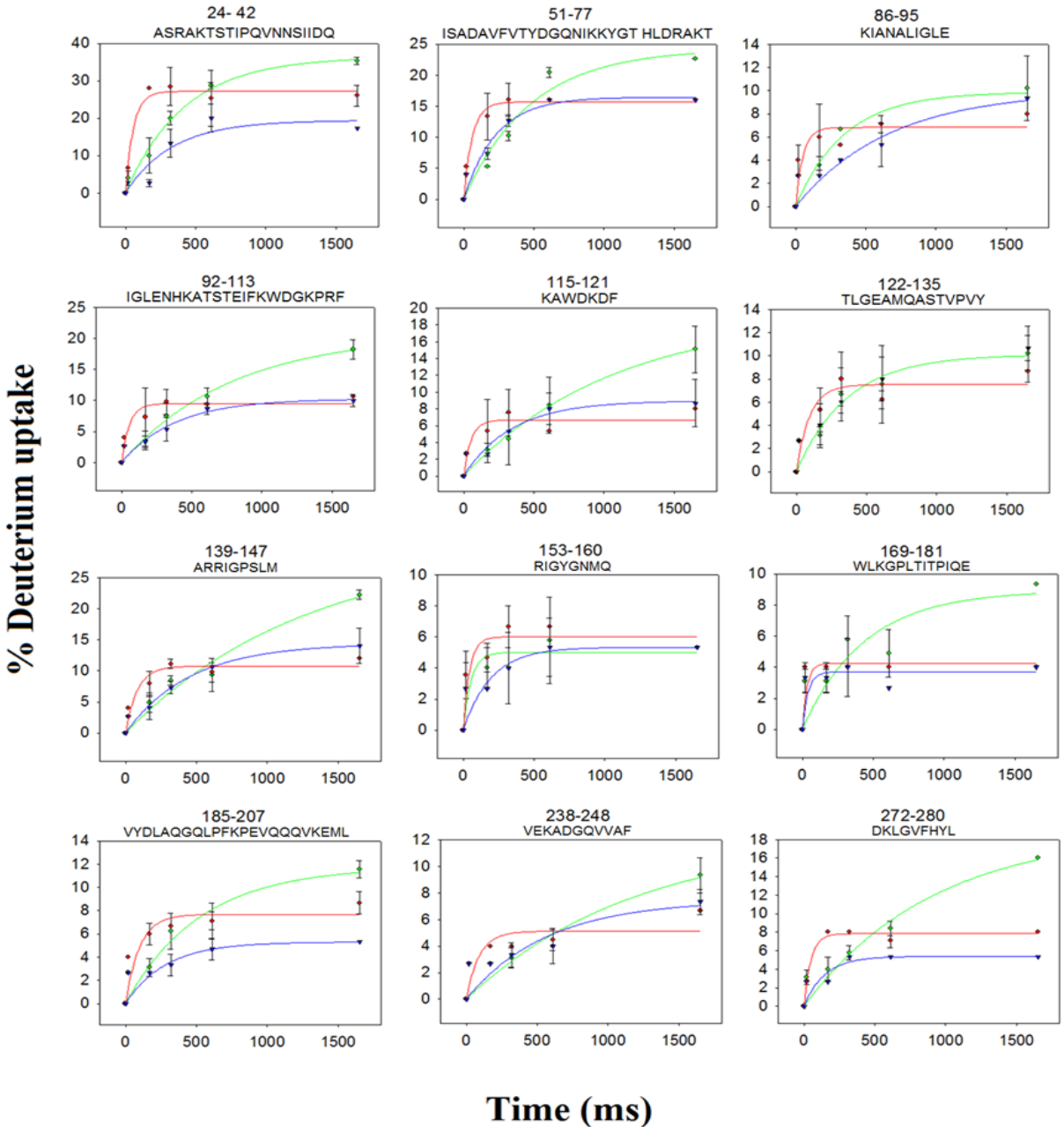

Figure 3.6 HDX kinetics plots for the 12 major OXA-58 peptides. **Green**: resting state OXA-58; **Red**: OXA-58-oxacillin reaction; **Blue**: OXA-58-impenem reaction. These peptides were observed in all three experiments. Conformational space explored by resting state enzyme is larger than with its reaction with oxacillin and imipenem because final deuterium uptake of green line is the highest. However, the rate at which the free enzyme explores its conformational space is lower than with its reaction with oxacillin because the initial rise of red curve is much sharper than that of green curve.

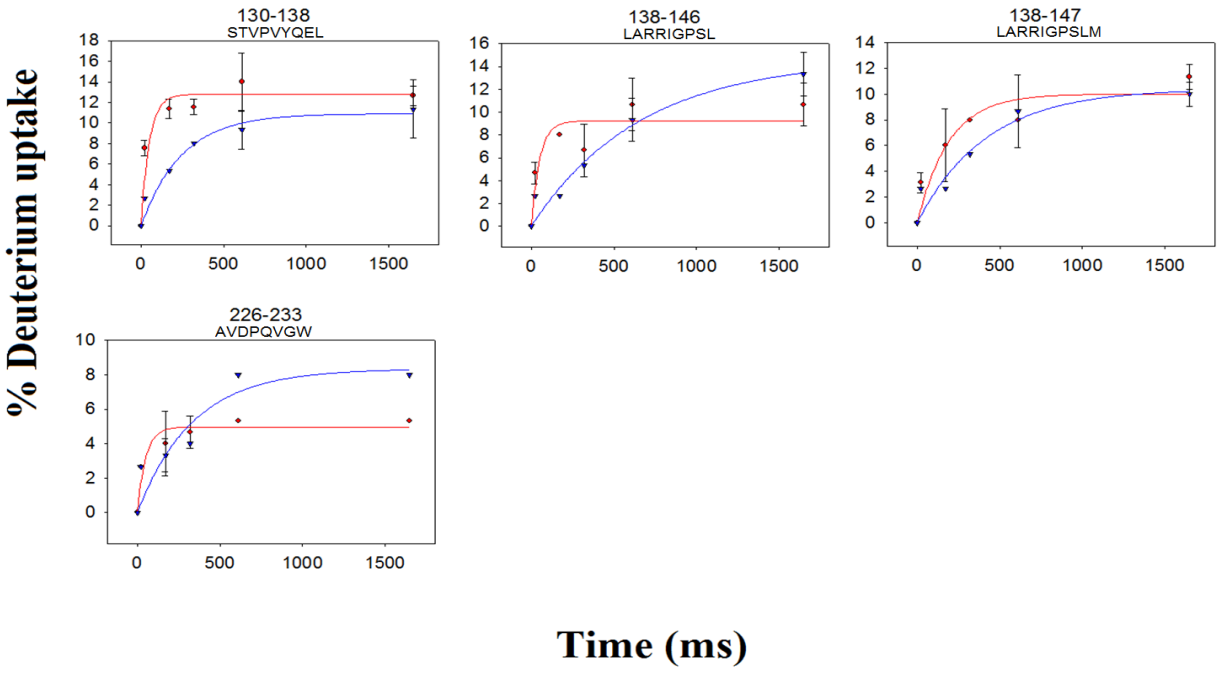

Figure 3.7 HDX kinetics plots for the OXA-58 peptides missing in free enzyme. Red: OXA-58-oxacillin reaction; **Blue**: OXA-58-impenem reaction. Here all peptides show similar final deuterium uptake (within error range) for OXA-58-oxacillin and OXA-58-imipenem reactions, with peptide 226-233 being an exception. The final uptake in this peptide is lower for good substrate oxacillin (red curve) than for poor substrate imipenem (blue curve). This indicates that when good substrate is present in the active site, the conformational space the enzyme explores at this region is restricted.

The HDX kinetics plots indicate that, for all peptides, the conformational space explored by the enzyme in the presence of good and poor substrates (red and blue respectively) is restricted to less than that of free enzyme (green), as indicated by a lower final deuterium uptake values. The fact that dynamics of the enzyme were restricted upon addition of the substrate suggests an induced fit model of ligand binding and catalysis.

While all other peptides exhibit similar final deuterium uptakes for oxacillin and imipenem runs, residues 86-95 and 226-233 did not. These regions show a lower deuterium

uptake for good substrate oxacillin than for poor substrate imipenem. This indicates that these regions of protein are directly linked to catalysis. Only when the good substrate is added to the enzyme, the conformational space the enzyme explores is restricted.

Another key observation made from the HDX kinetic plots is that OXA-58 explores the conformational space more rapidly while turning over good substrate oxacillin, i.e. the rate of deuterium uptake is faster. This is indicated by a sharp initial rise of red curve vs. the more subtly rising green and blue curves.

HDX profiles were generated next based on the deuterium uptake plots, using the OXA-58's crystal structure determined by Smith et al. as the template (PDB code 4OH0).[99] The changes free enzyme undergoes upon addition of the good substrate oxacillin are mapped in figure 3.8. Here the blue colour is indicative of the enzyme becoming more rigid upon addition of oxacillin and the green colour is indicative of no change in dynamics.

Figure 3.9 compares the deuterium uptake for OXA-58's reaction with substrates oxacillin with imipenem. Blue colour indicates that enzyme became more rigid when imipenem is present. Green colour indicates no change in dynamics and red suggests that region is more flexible when imipenem is present.

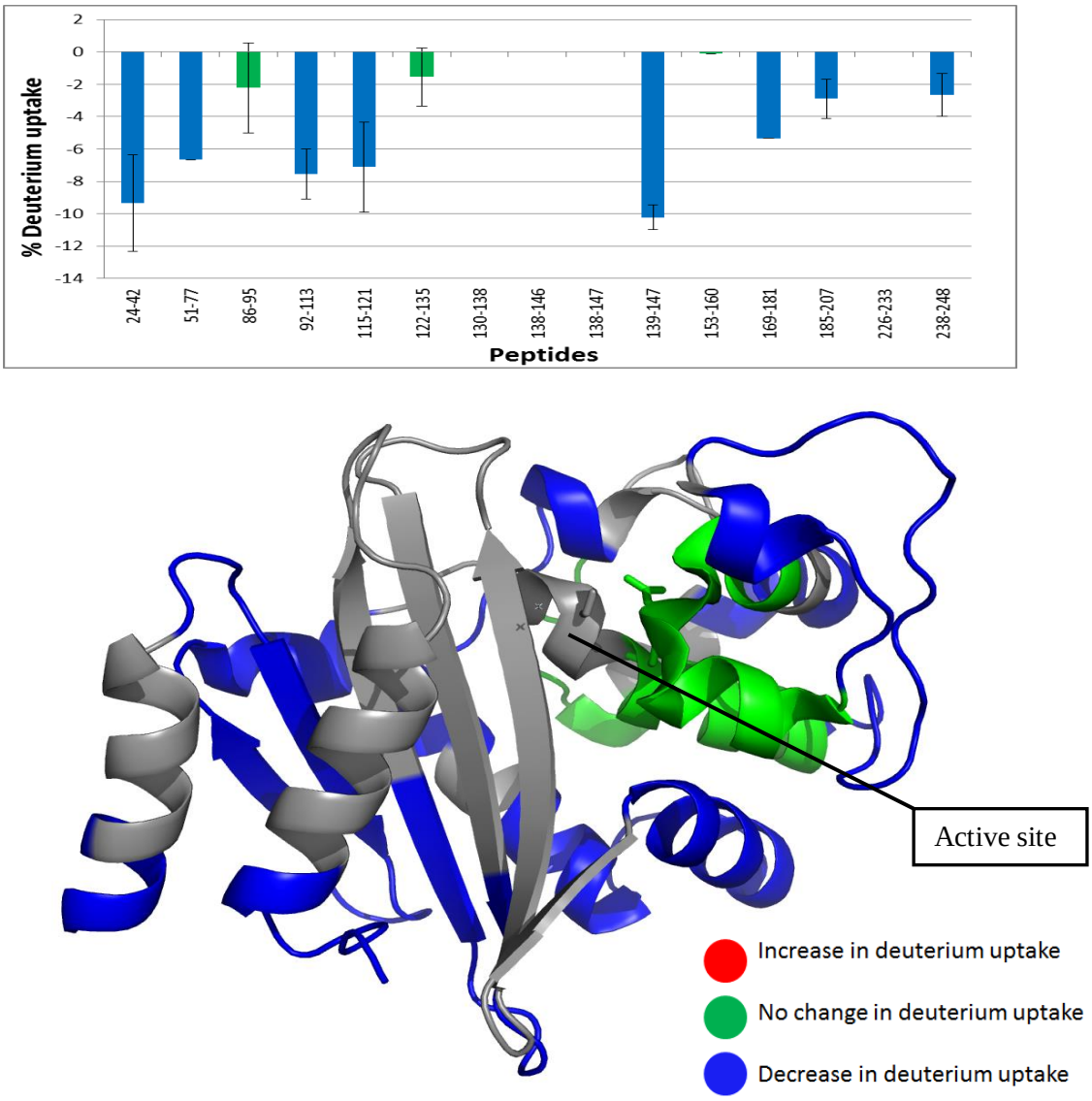

Figure 3.8 OXA-58 exchange profile comparing free enzyme and oxacillin-bound enzyme. OXA-58 structure determined by Smith et al. is used as the model (PDB code 4OH0).[99] The final deuterium uptake of apo (free) enzyme was subtracted from the final deuterium uptake of holo (with oxacillin) enzyme, to obtain the colour labels for the figure. **Top panel-** bar graph depicts deuterium uptake difference between apo and holo enzyme (oxacillin-bound minus free enzyme). **Bottom panel-** difference in deuterium uptake mapped on the 3D structure. **Blue** colour indicates that the enzyme becomes more structured in the presence of oxacillin. **Green** colour suggests that there is no change in dynamics. Active site is labeled on the structure as indicated.

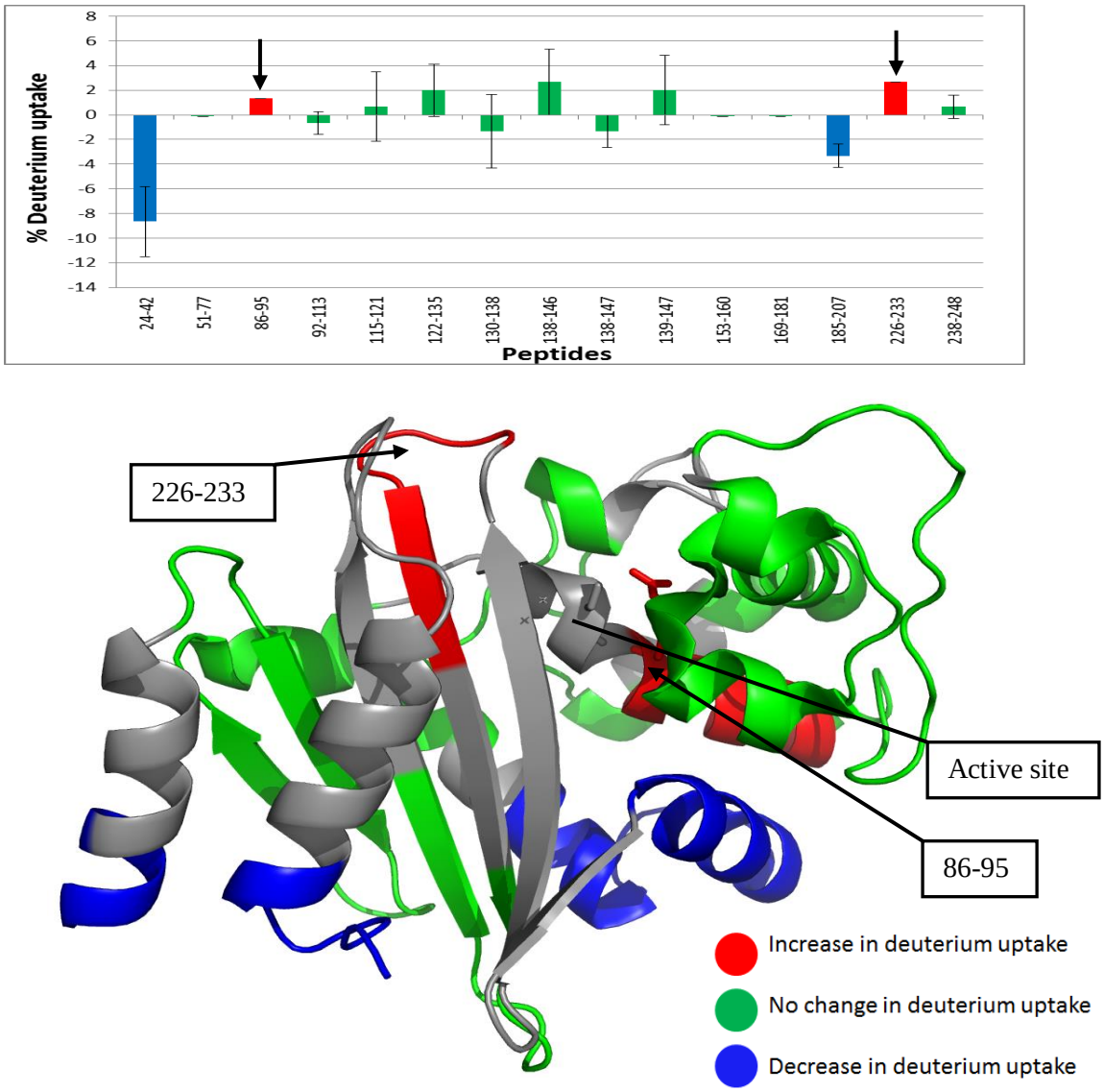

Figure 3.9 OXA-58 exchange profile comparing enzyme-oxacillin and enzyme-imipenem. OXA-58 structure determined by Smith et al. is used as the model (PDB code 4OH0).[99] The final deuterium uptake of enzyme-oxacillin reaction was subtracted from the final deuterium uptake of enzyme-imipenem reaction, to obtain the colour labels for the figure. **Top panel-** bar graph depicts deuterium uptake difference between two holo enzymes (imipenem-bound minus oxacillin-bound). **Bottom panel-** difference in deuterium uptake mapped on the 3D structure. **Blue** colour indicates that the enzyme becomes more structured in presence of poor substrate imipenem. **Green** colour implies no change in dynamics between substrates. **Red** colour suggests that particular peptide region is more flexible with imipenem. Peptide regions that show increase in uptake are labeled on structure.

Figure 3.9 shows the protein regions 86-95 and 226-233 highlighted in red. These portions are more flexible when poor substrate imipenem is present in the active site. It implies OXA-58's conformational space is restricted with good substrate oxacillin. These are the regions directly linked to catalysis. The fact that peptide 86-95 is near the enzyme active site (S83-XX-K86 motif) is suggestive of the enzyme becoming more rigid around oxacillin as it is converted to product.

Hydrophobic residue M225 of one loop interacts with hydrophobic residues F113 and F114 of a different loop. These interactions cause the enzyme to have a narrow tunnel like entry into the active site. The peptide 226-233 lies on one of these loops and is highlighted red since it is more dynamic in the presence of poor substrate imipenem. Since this peptide is more rigid in the good substrate oxacillin-enzyme reaction, it implies that the loop closes up on oxacillin during the catalysis phase. In conclusion, HDX data reveals that binding of substrate in the active site causes the enzyme to take an alternative pathway with restricted conformational space compared to substrate-free enzyme.

Chapter 4

Conclusion and Future Work

Wild-type and mutant OXA-58 β-lactamase's kinetic parameters were measured using ITC. It revealed that adding DTT to double mutant enzyme increases the turnover rate compared to when no DTT is added. DTT breaks the cross-link, which makes the enzyme more flexible and thus it turns the substrate over faster. For single mutants the common trend observed was that OXA-58 WT, M225A and F113Y were most catalytically efficient enzymes and F114I was the least catalytically efficient. Mutating the phenylalanine-114 residue to isoleucine hinders the catalytic activity of the enzyme significantly, if compared with the wild-type OXA-58. Imipenem is a poor substrate reflected in the data because OXA-58 WT and mutants were very inefficient in turning over imipenem into product.

Using HDX-MS it was possible to probe the dynamics of wild-type OXA-58 enzyme in its resting and catalytically active states as it turned over good substrate oxacillin and poor substrate imipenem. Substrate-bound enzyme showed a lower level of deuterium uptake vs. its substrate-free form. Since it was the region near the active site that becomes more structured when substrate is present, it suggests that the catalytic residues were alignment properly and enzyme closed up a bit when catalyzing the reaction. Since the binding of substrate lead to a restricted conformational space that the enzyme could explore, it is indicative of an induced fit model for catalysis linked dynamics.

ITC and UV-Vis spectroscopy studies conducted on the mutants revealed the importance of the point mutation in the functioning of the enzyme. The mutations such as F114I that lower the catalytic efficiency provide a gateway into drug development as these render the enzyme less

functional. The results are consistent because different instrumentation gave similar kinetic parameters trend i.e. the mutants that were proved most inefficient using ITC behaved the same way when tested with UV-Vis spectrometer.

Future work involves utilizing the power of mass spectrometry to its full potential in the field of enzymology. The technique of HDX-MS combined with the microfuidic chip provides reliable milli-second time scale information on enzyme dynamics. OXA-58's rate of deuterium uptake was faster in presence of substrate oxacillin, demonstrating that the dynamics were intensified. The substrate oxacillin also induced conformational change in OXA-58, making it more rigid. This work is a proof that using our setup enzyme dynamics can be studied and it is possible to determine the type of interaction an enzyme has with its ligand. Conformational selection model would not show any difference in the final deuterium uptake between free and ligand-bound enzyme, whereas induced fit model would (as observed for OXA-58).[73,100-106] Therefore, the type of conformational change in an enzyme can be studied simply based on the deuterium uptake trends, which is a great alternative to the more complicated techniques that exist for doing so. This work describes a method for classifying protein-ligand interactions for different enzymes under conformational selection or induced fit models.

Another application of this type of HDX technique would be to use it as a screening method for new and effective drugs targeting various enzymes. First a standard deuterium uptake profile can be obtained by mixing an enzyme with its known inhibitor. Then different drugs can be reacted with that specific enzyme one at a time and H/D exchange profiles can be obtained for them as well. Simply by comparing the deuterium exchange profile of all drugs with that of an inhibitor profile, it is possible to dinguish a 'good' drug from a 'bad' one. The HDX profile

obtained from reaction of enzyme-good drug should be similar to that of the enzyme-inhibtor profile, as this would indicate successful inhibtion of that enzyme.

References

(1) Brisou, J.; Prevot, A. R. [Studies on bacterial taxonomy. X. The revision of species under *Acromobacter* group]. *Annales de l'Institut Pasteur* **1954**, *86*, 722-728.

(2) Baumann, P.; Doudoroff, M.; Stanier, R. Y. A study of the *Moraxella* group. II. Oxidative-negative species (genus *Acinetobacter*). *Journal of Bacteriology* **1968**, *95*, 1520-1541.

(3) Doi, Y.; Kandiah, S.; Hariri, R. S.; Harrison, L. H. Natural history of multidrug-resistant Acinetobacter baumannii carriage in intensive care units. *Infection Control and Hospital Epidemiology : The Official Journal of the Society of Hospital Epidemiologists of America* **2012**, *33*, 642-643.

(4) Richet, H.; Fournier, P. E. Nosocomial infections caused by Acinetobacter baumannii: a major threat worldwide. *Infection Control and Hospital Epidemiology : The Official Journal of the Society of Hospital Epidemiologists of America* **2006**, *27*, 645-646.

(5) Vallenet, D.; Nordmann, P.; Barbe, V.; Poirel, L.; Mangenot, S.; Bataille, E.; Dossat, C.; Gas, S.; Kreimeyer, A.; Lenoble, P.; Oztas, S.; Poulain, J.; Segurens, B.; Robert, C.; Abergel, C.; Claverie, J. M.; Raoult, D.; Medigue, C.; Weissenbach, J.; Cruveiller, S. Comparative analysis of Acinetobacters: three genomes for three lifestyles. *PloS One* **2008**, *3*, e1805.

(6) Fournier, P. E.; Richet, H. The epidemiology and control of *Acinetobacter baumannii* in health care facilities. *Clinical Infectious Diseases : An Official Publication of the Infectious Diseases Society of America* **2006**, *42*, 692-699.

(7) Doughari, H. J.; Ndakidemi, P. A.; Human, I. S.; Benade, S. The ecology, biology and pathogenesis of *Acinetobacter* spp.: an overview. *Microbes and Environments / JSME* **2011**, *26*, 101-112.

(8) Spratt, B. G. Properties of the penicillin-binding proteins of *Escherichia coli* K12. *European Journal of Biochemistry / FEBS* **1977**, *72*, 341-352.

(9) Ghuysen, J. M. Molecular structures of penicillin-binding proteins and β-lactamases. *Trends in Microbiology* **1994**, *2*, 372-380.

(10) Dzhekieva, L.; Kumar, I.; Pratt, R. F. Inhibition of bacterial DD-peptidases (penicillin-binding proteins) in membranes and in vivo by peptidoglycan-mimetic boronic acids. *Biochemistry* **2012**, *51*, 2804-2811.

(11) Essack, S. Y. The development of β-lactam antibiotics in response to the evolution of β-lactamases. *Pharmaceutical Research* **2001**, *18*, 1391-1399.

(12) Siu, L. K. Antibiotics: action and resistance in gram-negative bacteria. *Journal of Microbiology, Immunology, and Infection = Wei mian yu gan ran za zhi* **2002**, *35*, 1-11.

(13) Dalhoff, A.; Thomson, C. J. The art of fusion: from penams and cephems to penems. *Chemotherapy* **2003**, *49*, 105-120.

(14) Ehmann, D. E.; Jahic, H.; Ross, P. L.; Gu, R. F.; Hu, J.; Kern, G.; Walkup, G. K.; Fisher, S. L. Avibactam is a covalent, reversible, non-β-lactam β-lactamase inhibitor. *Proceedings of the National Academy of Sciences of the United States of America* **2012**, *109*, 11663-11668.

(15) Holten, K. B.; Onusko, E. M. Appropriate prescribing of oral β-lactam antibiotics. *American Family Physician* **2000**, *62*, 611-620.

(16) Tipper, D. J.; Strominger, J. L. Mechanism of action of penicillins: a proposal based on their structural similarity to acyl-D-alanyl-D-alanine. *Proceedings of the National Academy of Sciences of the United States of America* **1965**, *54*, 1133-1141.

(17) Guignard, B.; Entenza, J. M.; Moreillon, P. β-lactams against methicillin-resistant *Staphylococcus aureus*. *Current Opinion in Pharmacology* **2005**, *5*, 479-489.

(18) Ghuysen, J. M. Serine β-lactamases and penicillin-binding proteins. *Annual Review of Microbiology* **1991**, *45*, 37-67.

(19) Zeng, X.; Lin, J. B-lactamase induction and cell wall metabolism in Gram-negative bacteria. *Frontiers in Microbiology* **2013**, *4*, 128.

(20) Woodward, R. B. Penems and related substances. *Philosophical Transactions of the Royal Society of London. Series B, Biological Sciences* **1980**, *289*, 239-250.

(21) Dalhoff, A.; Janjic, N.; Echols, R. Redefining penems. *Biochemical Pharmacology* **2006**, *71*, 1085-1095.

(22) Hujer, A. M.; Kania, M.; Gerken, T.; Anderson, V. E.; Buynak, J. D.; Ge, X.; Caspers, P.; Page, M. G.; Rice, L. B.; Bonomo, R. A. Structure-activity relationships of different β-lactam antibiotics against a soluble form of *Enterococcus faecium* PBP5, a type II bacterial transpeptidase. *Antimicrobial Agents and Chemotherapy* **2005**, *49*, 612-618.

(23) Bailon-Perez, M. I.; Garcia-Campana, A. M.; del Olmo-Iruela, M.; Gamiz-Gracia, L.; Cruces-Blanco, C. Trace determination of 10 β-lactam antibiotics in environmental and food samples by capillary liquid chromatography. *Journal of Chromatography. A* **2009**, *1216*, 8355-8361.

(24) Lee, M.; Hesek, D.; Mobashery, S. A practical synthesis of nitrocefin. *The Journal of Organic Chemistry* **2005**, *70*, 367-369.

(25) Unal, S.; Garcia-Rodriguez, J. A. Activity of meropenem and comparators against *Pseudomonas aeruginosa* and *Acinetobacter* spp. isolated in the MYSTIC Program, 2002-2004. *Diagnostic Microbiology and Infectious Disease* **2005**, *53*, 265-271.

(26) Su, C. H.; Wang, J. T.; Hsiung, C. A.; Chien, L. J.; Chi, C. L.; Yu, H. T.; Chang, F. Y.; Chang, S. C. Increase of carbapenem-resistant *Acinetobacter baumannii* infection in acute care hospitals in Taiwan: association with hospital antimicrobial usage. *PloS One* **2012**, *7*, e37788.

(27) Perez, F.; Hujer, A. M.; Hujer, K. M.; Decker, B. K.; Rather, P. N.; Bonomo, R. A. Global challenge of multidrug-resistant *Acinetobacter baumannii*. *Antimicrobial Agents and Chemotherapy* **2007**, *51*, 3471-3484.

(28) Poirel, L.; Nordmann, P. Carbapenem resistance in *Acinetobacter baumannii*: mechanisms and epidemiology. *Clinical Microbiology and Infection : The Official Publication of the European Society of Clinical Microbiology and Infectious Diseases* **2006**, *12*, 826-836.

(29) Poirel, L.; Bonnin, R. A.; Nordmann, P. Genetic basis of antibiotic resistance in pathogenic *Acinetobacter* species. *IUBMB Life* **2011**, *63*, 1061-1067.

(30) Livermore, D. M. β-Lactamases in laboratory and clinical resistance. *Clinical Microbiology Reviews* **1995**, *8*, 557-584.

(31) Joris, B.; Ghuysen, J. M.; Dive, G.; Renard, A.; Dideberg, O.; Charlier, P.; Frere, J. M.; Kelly, J. A.; Boyington, J. C.; Moews, P. C.; et al. The active-site-serine penicillin-recognizing enzymes as members of the *Streptomyces* R61 DD-peptidase family. *The Biochemical Journal* **1988**, *250*, 313-324.

(32) Frere, J. M.; Duez, C.; Ghuysen, J. M.; Vandekerkhove, J. Occurrence of a serine residue in the penicillin-binding site of the exocellular DD-carboxy-peptidase-transpeptidase from *Streptomyces* R61. *FEBS Letters* **1976**, *70*, 257-260.

(33) Bush, K.; Jacoby, G. A.; Medeiros, A. A. A functional classification scheme for β-lactamases and its correlation with molecular structure. *Antimicrobial Agents and Chemotherapy* **1995**, *39*, 1211-1233.

(34) Bush, K.; Jacoby, G. A. Updated functional classification of β-lactamases. *Antimicrobial Agents and Chemotherapy* **2010**, *54*, 969-976.

(35) Livermore, D. M. β-lactamase-mediated resistance and opportunities for its control. *The Journal of Antimicrobial Chemotherapy* **1998**, *41 Suppl D*, 25-41.

(36) Ambler, R. P.; Coulson, A. F.; Frere, J. M.; Ghuysen, J. M.; Joris, B.; Forsman, M.; Levesque, R. C.; Tiraby, G.; Waley, S. G. A standard numbering scheme for the class A β-lactamases. *The Biochemical Journal* **1991**, *276 (Pt 1)*, 269-270.

(37) Evans, B. A.; Amyes, S. G. OXA β-lactamases. *Clinical Microbiology Reviews* **2014**, *27*, 241-263.

(38) Bonfiglio, G.; Russo, G.; Nicoletti, G. Recent developments in carbapenems. *Expert Opinion on Investigational Drugs* **2002**, *11*, 529-544.

(39) Queenan, A. M.; Bush, K. Carbapenemases: the versatile β-lactamases. *Clinical Microbiology Reviews* **2007**, *20*, 440-458.

(40) Walsh, T. R. Clinically significant carbapenemases: an update. *Current Opinion in Infectious Diseases* **2008**, *21*, 367-371.

(41) Poirel, L.; Pitout, J. D.; Nordmann, P. Carbapenemases: molecular diversity and clinical consequences. *Future Microbiology* **2007**, *2*, 501-512.

(42) Marque, S.; Poirel, L.; Heritier, C.; Brisse, S.; Blasco, M. D.; Filip, R.; Coman, G.; Naas, T.; Nordmann, P. Regional occurrence of plasmid-mediated carbapenem-hydrolyzing oxacillinase OXA-58 in *Acinetobacter* spp. in Europe. *Journal of Clinical Microbiology* **2005**, *43*, 4885-4888.

(43) Zarrilli, R.; Giannouli, M.; Tomasone, F.; Triassi, M.; Tsakris, A. Carbapenem resistance in *Acinetobacter baumannii*: the molecular epidemic features of an emerging problem in health care facilities. *Journal of Infection in Developing Countries* **2009**, *3*, 335-341.

(44) Heritier, C.; Dubouix, A.; Poirel, L.; Marty, N.; Nordmann, P. A nosocomial outbreak of *Acinetobacter baumannii* isolates expressing the carbapenem-hydrolysing oxacillinase OXA-58. *The Journal of Antimicrobial Chemotherapy* **2005**, *55*, 115-118.

(45) Poirel, L.; Heritier, C.; Tolun, V.; Nordmann, P. Emergence of oxacillinase-mediated resistance to imipenem in *Klebsiella pneumoniae*. *Antimicrobial Agents and Chemotherapy* **2004**, *48*, 15-22.

(46) Brown, S.; Amyes, S. OXA (β)-lactamases in *Acinetobacter*: the story so far. *The Journal of Antimicrobial Chemotherapy* **2006**, *57*, 1-3.

(47) Walther-Rasmussen, J.; Hoiby, N. OXA-type carbapenemases. *The Journal of Antimicrobial Chemotherapy* **2006**, *57*, 373-383.

(48) Higgins, P. G.; Dammhayn, C.; Hackel, M.; Seifert, H. Global spread of carbapenem-resistant *Acinetobacter baumannii*. *The Journal of Antimicrobial Chemotherapy* **2010**, *65*, 233-238.

(49) Santillana, E.; Beceiro, A.; Bou, G.; Romero, A. Crystal structure of the carbapenemase OXA-24 reveals insights into the mechanism of carbapenem hydrolysis.

Proceedings of the National Academy of Sciences of the United States of America **2007**, *104*, 5354-5359.

(50) Bou, G.; Santillana, E.; Sheri, A.; Beceiro, A.; Sampson, J. M.; Kalp, M.; Bethel, C. R.; Distler, A. M.; Drawz, S. M.; Pagadala, S. R.; van den Akker, F.; Bonomo, R. A.; Romero, A.; Buynak, J. D. Design, synthesis, and crystal structures of 6-alkylidene-2'-substituted penicillanic acid sulfones as potent inhibitors of *Acinetobacter baumannii* OXA-24 carbapenemase. *Journal of the American Chemical Society* **2010**, *132*, 13320-13331.

(51) Schneider, K. D.; Ortega, C. J.; Renck, N. A.; Bonomo, R. A.; Powers, R. A.; Leonard, D. A. Structures of the class D carbapenemase OXA-24 from *Acinetobacter baumannii* in complex with doripenem. *Journal of Molecular Biology* **2011**, *406*, 583-594.

(52) Docquier, J. D.; Calderone, V.; De Luca, F.; Benvenuti, M.; Giuliani, F.; Bellucci, L.; Tafi, A.; Nordmann, P.; Botta, M.; Rossolini, G. M.; Mangani, S. Crystal structure of the OXA-48 β-lactamase reveals mechanistic diversity among class D carbapenemases. *Chemistry & Biology* **2009**, *16*, 540-547.

(53) Poirel, L.; Marque, S.; Heritier, C.; Segonds, C.; Chabanon, G.; Nordmann, P. OXA-58, a novel class D {beta}-lactamase involved in resistance to carbapenems in *Acinetobacter baumannii*. *Antimicrobial Agents and Chemotherapy* **2005**, *49*, 202-208.

(54) Verma, V.; Testero, S. A.; Amini, K.; Wei, W.; Liu, J.; Balachandran, N.; Monoharan, T.; Stynes, S.; Kotra, L. P.; Golemi-Kotra, D. Hydrolytic mechanism of OXA-58 enzyme, a carbapenem-hydrolyzing class D β-lactamase from *Acinetobacter baumannii*. *The Journal of Biological Chemistry* **2011**, *286*, 37292-37303.

(55) Vercheval, L.; Bauvois, C.; di Paolo, A.; Borel, F.; Ferrer, J. L.; Sauvage, E.; Matagne, A.; Frere, J. M.; Charlier, P.; Galleni, M.; Kerff, F. Three factors that modulate the

activity of class D β-lactamases and interfere with the post-translational carboxylation of Lys70. *The Biochemical Journal* **2010**, *432*, 495-504.

(56) Golemi, D.; Maveyraud, L.; Vakulenko, S.; Samama, J. P.; Mobashery, S. Critical involvement of a carbamylated lysine in catalytic function of class D β-lactamases. *Proceedings of the National Academy of Sciences of the United States of America* **2001**, *98*, 14280-14285.

(57) Pierce, M. M.; Raman, C. S.; Nall, B. T. Isothermal titration calorimetry of protein-protein interactions. *Methods* **1999**, *19*, 213-221.

(58) Holdgate, G. Isothermal titration calorimetry and differential scanning calorimetry. *Methods in Molecular Biology* **2009**, *572*, 101-133.

(59) O'Brien, R.; Haq, I.: Applications of Biocalorimetry: Binding, Stability and Enzyme Kinetics. In *Biocalorimetry 2*; John Wiley & Sons, Ltd, 2005; pp 1-34.

(60) Mazzei, L.; Ciurli, S.; Zambelli, B. Hot biological catalysis: isothermal titration calorimetry to characterize enzymatic reactions. *Journal of Visualized Experiments : JoVE* **2014**.

(61) Freyer, M. W.; Lewis, E. A. Isothermal titration calorimetry: experimental design, data analysis, and probing macromolecule/ligand binding and kinetic interactions. *Methods in Cell Biology* **2008**, *84*, 79-113.

(62) Brown, A. Analysis of cooperativity by isothermal titration calorimetry. *International Journal of Molecular Sciences* **2009**, *10*, 3457-3477.

(63) Todd, M. J.; Gomez, J. Enzyme kinetics determined using calorimetry: a general assay for enzyme activity? *Analytical Biochemistry* **2001**, *296*, 179-187.

(64) Demarse, N.; Killian, M.; Hansen, L.; Quinn, C.: Determining Enzyme Kinetics via Isothermal Titration Calorimetry. In *Enzyme Engineering*; Samuelson, J. C., Ed.; Methods in Molecular Biology; Humana Press, 2013; Vol. 978; pp 21-30.

(65) Frauenfelder, H.; Sligar, S. G.; Wolynes, P. G. The energy landscapes and motions of proteins. *Science* **1991**, *254*, 1598-1603.

(66) Lindorff-Larsen, K.; Best, R. B.; Depristo, M. A.; Dobson, C. M.; Vendruscolo, M. Simultaneous determination of protein structure and dynamics. *Nature* **2005**, *433*, 128-132.

(67) Pocker, Y.; Biswas, S. B. Conformational dynamics of insulin in solution. Circular dichroic studies. *Biochemistry* **1980**, *19*, 5043-5049.

(68) Henzler-Wildman, K.; Kern, D. Dynamic personalities of proteins. *Nature* **2007**, *450*, 964-972.

(69) Pan, J.; Han, J.; Borchers, C. H.; Konermann, L. Hydrogen/deuterium exchange mass spectrometry with top-down electron capture dissociation for characterizing structural transitions of a 17 kDa protein. *Journal of the American Chemical Society* **2009**, *131*, 12801-12808.

(70) Benkovic, S. J.; Hammes-Schiffer, S. A perspective on enzyme catalysis. *Science* **2003**, *301*, 1196-1202.

(71) Mulder, F. A.; Mittermaier, A.; Hon, B.; Dahlquist, F. W.; Kay, L. E. Studying excited states of proteins by NMR spectroscopy. *Nature Structural Biology* **2001**, *8*, 932-935.

(72) Kern, D.; Zuiderweg, E. R. The role of dynamics in allosteric regulation. *Current Opinion in Structural Biology* **2003**, *13*, 748-757.

(73) Eisenmesser, E. Z.; Millet, O.; Labeikovsky, W.; Korzhnev, D. M.; Wolf-Watz, M.; Bosco, D. A.; Skalicky, J. J.; Kay, L. E.; Kern, D. Intrinsic dynamics of an enzyme underlies catalysis. *Nature* **2005**, *438*, 117-121.

(74) Englander, S. W.; Sosnick, T. R.; Englander, J. J.; Mayne, L. Mechanisms and uses of hydrogen exchange. *Current Opinion in Structural Biology* **1996**, *6*, 18-23.

(75) Englander, S. W. Protein folding intermediates and pathways studied by hydrogen exchange. *Annual Review of Biophysics and Biomolecular Structure* **2000**, *29*, 213-238.

(76) Konermann, L.; Pan, J.; Liu, Y. H. Hydrogen exchange mass spectrometry for studying protein structure and dynamics. *Chemical Society Reviews* **2011**, *40*, 1224-1234.

(77) Wagner, G.; Wuthrich, K. Amide protein exchange and surface conformation of the basic pancreatic trypsin inhibitor in solution. Studies with two-dimensional nuclear magnetic resonance. *Journal of Molecular Biology* **1982**, *160*, 343-361.

(78) Ferentz, A. E.; Wagner, G. NMR spectroscopy: a multifaceted approach to macromolecular structure. *Quarterly Reviews of Biophysics* **2000**, *33*, 29-65.

(79) Ohki, S.; Eto, M.; Kariya, E.; Hayano, T.; Hayashi, Y.; Yazawa, M.; Brautigan, D.; Kainosho, M. Solution NMR structure of the myosin phosphatase inhibitor protein CPI-17 shows phosphorylation-induced conformational changes responsible for activation. *Journal of Molecular Biology* **2001**, *314*, 839-849.

(80) Tolman, J. R.; Flanagan, J. M.; Kennedy, M. A.; Prestegard, J. H. NMR evidence for slow collective motions in cyanometmyoglobin. *Nature Structural Biology* **1997**, *4*, 292-297.

(81) Mori, S.; Abeygunawardana, C.; Johnson, M. O.; van Zijl, P. C. Improved sensitivity of HSQC spectra of exchanging protons at short interscan delays using a new fast HSQC (FHSQC) detection scheme that avoids water saturation. *Journal of Magnetic Resonance. Series B* **1995**, *108*, 94-98.

(82) Marcsisin, S. R.; Engen, J. R. Hydrogen exchange mass spectrometry: what is it and what can it tell us? *Analytical and Bioanalytical Chemistry* **2010**, *397*, 967-972.

(83) Wales, T. E.; Engen, J. R. Hydrogen exchange mass spectrometry for the analysis of protein dynamics. *Mass Spectrometry Reviews* **2006**, *25*, 158-170.

(84) Ferguson, P. L.; Pan, J.; Wilson, D. J.; Dempsey, B.; Lajoie, G.; Shilton, B.; Konermann, L. Hydrogen/deuterium scrambling during quadrupole time-of-flight MS/MS analysis of a zinc-binding protein domain. *Analytical Chemistry* **2007**, *79*, 153-160.

(85) Jorgensen, T. J.; Bache, N.; Roepstorff, P.; Gardsvoll, H.; Ploug, M. Collisional activation by MALDI tandem time-of-flight mass spectrometry induces intramolecular migration of amide hydrogens in protonated peptides. *Molecular & Cellular Proteomics : MCP* **2005**, *4*, 1910-1919.

(86) Hoerner, J. K.; Xiao, H.; Dobo, A.; Kaltashov, I. A. Is there hydrogen scrambling in the gas phase? Energetic and structural determinants of proton mobility within protein ions. *Journal of the American Chemical Society* **2004**, *126*, 7709-7717.

(87) Zhang, Z.; Smith, D. L. Determination of amide hydrogen exchange by mass spectrometry: a new tool for protein structure elucidation. *Protein Science* **1993**, *2*, 522-531.

(88) Krishna, M. M.; Hoang, L.; Lin, Y.; Englander, S. W. Hydrogen exchange methods to study protein folding. *Methods* **2004**, *34*, 51-64.

(89) Engen, J. R.; Smithgall, T. E.; Gmeiner, W. H.; Smith, D. L. Identification and localization of slow, natural, cooperative unfolding in the hematopoietic cell kinase SH3 domain by amide hydrogen exchange and mass spectrometry. *Biochemistry* **1997**, *36*, 14384-14391.

(90) Deng, Y.; Zhang, Z.; Smith, D. L. Comparison of continuous and pulsed labeling amide hydrogen exchange/mass spectrometry for studies of protein dynamics. *Journal of the American Society for Mass Spectrometry* **1999**, *10*, 675-684.

(91) Simmons, D. A.; Dunn, S. D.; Konermann, L. Conformational dynamics of partially denatured myoglobin studied by time-resolved electrospray mass spectrometry with online hydrogen-deuterium exchange. *Biochemistry* **2003**, *42*, 5896-5905.

(92) Kebarle, P.; Verkerk, U. H. Electrospray: from ions in solution to ions in the gas phase, what we know now. *Mass Spectrometry Reviews* **2009**, *28*, 898-917.

(93) Kebarle, P. A brief overview of the present status of the mechanisms involved in electrospray mass spectrometry. *Journal of mass spectrometry : JMS* **2000**, *35*, 804-817.

(94) Chernushevich, I. V.; Loboda, A. V.; Thomson, B. A. An introduction to quadrupole-time-of-flight mass spectrometry. *Journal of Mass Spectrometry* **2001**, *36*, 849-865.

(95) Poduch, E.; Bello, A. M.; Tang, S.; Fujihashi, M.; Pai, E. F.; Kotra, L. P. Design of inhibitors of orotidine monophosphate decarboxylase using bioisosteric replacement and determination of inhibition kinetics. *Journal of Medicinal Chemistry* **2006**, *49*, 4937-4945.

(96) Rob, T.; Wilson, D. J. A versatile microfluidic chip for millisecond time-scale kinetic studies by electrospray mass spectrometry. *Journal of the American Society for Mass Spectrometry* **2009**, *20*, 124-130.

(97) Liuni, P.; Rob, T.; Wilson, D. J. A microfluidic reactor for rapid, low-pressure proteolysis with on-chip electrospray ionization. *Rapid Communications in Mass Spectrometry* **2010**, *24*, 315-320.

(98) Rob, T.; Liuni, P.; Gill, P. K.; Zhu, S.; Balachandran, N.; Berti, P. J.; Wilson, D. J. Measuring dynamics in weakly structured regions of proteins using microfluidics-enabled subsecond H/D exchange mass spectrometry. *Analytical Chemistry* **2012**, *84*, 3771-3779.

(99) Smith, C. A.; Antunes, N. T.; Toth, M.; Vakulenko, S. B. Crystal structure of carbapenemase OXA-58 from Acinetobacter baumannii. *Antimicrobial Agents and Chemotherapy* **2014**, *58*, 2135-2143.

(100) Eisenmesser, E. Z.; Bosco, D. A.; Akke, M.; Kern, D. Enzyme dynamics during catalysis. *Science* **2002**, *295*, 1520-1523.

(101) Henzler-Wildman, K. A.; Thai, V.; Lei, M.; Ott, M.; Wolf-Watz, M.; Fenn, T.; Pozharski, E.; Wilson, M. A.; Petsko, G. A.; Karplus, M.; Hubner, C. G.; Kern, D. Intrinsic motions along an enzymatic reaction trajectory. *Nature* **2007**, *450*, 838-844.

(102) Liu, Y. H.; Konermann, L. Enzyme conformational dynamics during catalysis and in the 'resting state' monitored by hydrogen/deuterium exchange mass spectrometry. *FEBS Letters* **2006**, *580*, 5137-5142.

(103) Wolf-Watz, M.; Thai, V.; Henzler-Wildman, K.; Hadjipavlou, G.; Eisenmesser, E. Z.; Kern, D. Linkage between dynamics and catalysis in a thermophilic-mesophilic enzyme pair. *Nature Structural & Molecular Biology* **2004**, *11*, 945-949.

(104) Henzler-Wildman, K. A.; Lei, M.; Thai, V.; Kerns, S. J.; Karplus, M.; Kern, D. A hierarchy of timescales in protein dynamics is linked to enzyme catalysis. *Nature* **2007**, *450*, 913-916.

(105) Masterson, L. R.; Cheng, C.; Yu, T.; Tonelli, M.; Kornev, A.; Taylor, S. S.; Veglia, G. Dynamics connect substrate recognition to catalysis in protein kinase A. *Nature Chemical Biology* **2010**, *6*, 821-828.

(106) Jensen, K. S.; Winther, J. R.; Teilum, K. Millisecond dynamics in glutaredoxin during catalytic turnover is dependent on substrate binding and absent in the resting states. *Journal of the American Chemical Society* **2011**, *133*, 3034-3042.

Appendix

Sample calculation is shown for determining reaction time, which depends on the length the protein capillary is pulled back.

Calculation shown for inner protein capillary pulled back 1 mm

Radius of outer metal capillary, r_2 = Diameter / 2 = 158.75 μm / 2 = 76.5μm

Radius of inner glass capillary, r_1 = Diameter / 2 = 153 μm / 2 = 79.375 μm

Calculate mixing region volume and total flow rate:

Length of mixing region = 2 mm $1\ \mu m^3 = 1 \times 10^{-6}$ nL

Volume = $\pi\ (r_2^2 - r_1^2) \times 2$ mm

$= \pi\ [(79.375\ \mu m)^2 - (76.5\ \mu m)^2] \times 2\ mm \times (1000\ \mu m / 1\ mm)$

$= 2815750.59\ \mu m^3 = 2.815751$ nL

Total flow rate = Protein flow rate + D_2O flow rate

= 2 μL/min + 6 μL/min = 8 μL/min = 133.33 nL/sec

Calculate reaction time in milliseconds:

For 0 mm, Time (ms) = Volume of mixing region / Total flow rate

= [2.815751 nL / (133.33 nL/sec)] x 1000 ms / 1 s

= 20 ms = dead time

For 1 mm, Volume = π (79.375 μm)^2 x 1 mm x (1000 μm / 1 mm)

= 19793260.9 μm^3 = 19.79 nL

Time (ms) = (Volume of mixing region / Total flow rate) + dead volume

= [(19.79 nL / 133.33 nL/sec) x 1000 ms/ 1sec] + 21 ms

= 170 ms

For 1 mm pullback, the actual reaction time is 170 milliseconds.